Universität
Konstanz

Higher harmonics in colloid rheology

Master thesis

Rabea Seyboldt

23.10.2013

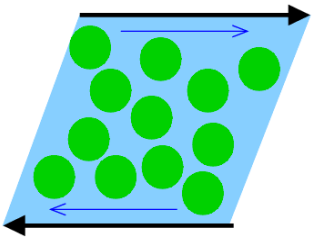

1. Gutachter & Betreuer: Prof. Dr. Matthias Fuchs
2. Gutachter: Dr. Thomas Voigtmann

Zusammenfassung

In der vorliegenden Arbeit wird ein schematischer Ansatz der Modenkopplungstheorie in zwei Zeitvariablen für kleine oszillatorische Scherauslenkungen mit Frequenz ω analysiert. Mithilfe einer Taylorentwicklung der Dichte-Korrelationsfunktion werden Störterme zweiter Ordnung der Lösung im Equilibrium hergeleitet und ihr Langzeitverhalten analysiert. Die Integro-Differentialgleichungen, welche die Störterme beschreiben, werden zudem numerisch gelöst und erfolgreich mit den analytischen Ergebnissen verglichen.

Die zeitabhängigen Taylorkoeffizienten weisen ein unterschiedliches Verhalten, abhängig vom Abstand ϵ des Systems vom Glasübergang, auf. In einer Flüssigkeit, $\epsilon < 0$, zerfällt die Lösung für lange Zeiten zu Null. Für endliche Zeiten oszilliert sie mit abnehmender Amplitude und Frequenzen ω und 2ω um eine langsamere Funktion, welche ein Minimum entwickelt, bevor sie gegen Null konvergiert. Der Verlauf gegen das Minimum kann mit einem Potenzgesetz mit Exponent $1/3$ beschrieben werden. Bei Annäherung an den Glasübergang geht der Wert des Minimums gegen minus Unendlich, so dass die Lösung direkt am Glasübergang ($\epsilon = 0$) entsprechend dem Potenzgesetz divergiert. Im Glas mit $\epsilon > 0$ oszilliert die Langzeitlösung mit endlicher Amplitude um einen endlichen Offset. Die Amplitude ist dabei frequenzabhängig und kann über die Fouriertransformierte der Equilibriumslösung bestimmt werden. Für kleine Frequenzen bildet die Amplitude ein Plateau mit dem Wert des Limes $\omega \to 0$. Der Grenzwert und die Frequenz, bei der das Plateau beginnt, ist dabei ϵ-abhängig. Für große Frequenzen ist die Amplitude nur schwach abhängig von ϵ, aber abhängig von der Frequenz ω.

Ein Vergleich mit dem vollen schematischen Modell zeigt eine gute Übereinstimmung mit der Taylor-Näherung für mittellange Zeiten. Für lange Zeiten hingegen scheint die volle Lösung zu zerfallen. Dies findet sich in der Taylor-Lösung nur direkt am Glasübergang für $\epsilon = 0$. Erste Ansätze, ein Skalengesetz für den Zerfall des Korrelators zu finden, werden vorgestellt.

Die Taylor-Näherung kann genutzt werden, um eine Formel für die Scherspannung herzuleiten. Dies ermöglicht es, den ersten höheren harmonischen Beitrag zu bestimmen. Ein Vergleich des ersten höheren harmonischen Bietrags mit experimentellen Daten bildet den Abschluss der Arbeit

Abstract

In this thesis we analyze a schematic Mode-Coupling Theory in two time variables for small amplitude oscillatory shear with frequency ω. We derive the second order Taylor approximation for the density correlator and formulas for its long-time behavior. We also numerically solve the resulting equations, thus confirming the analytic results.

We find that the solutions for the perturbation of the equilibrium correlator behave differently depending on the distance to the glass transition ϵ. In a liquid, $\epsilon < 0$, the solutions decay to zero for long times, with a minimum for intermediate times, and an overlying decaying oscillation with frequencies ω and 2ω. We find a power-law governing the decay towards the minimum. Approaching the glass transition, the value of the minimum goes towards minus infinity, such that, at the glass transition, $\epsilon = 0$, we get a diverging power-law solution with apparent exponent $1/3$ and an overlying finite oscillation with frequencies ω and 2ω for all times. In the glass for $\epsilon > 0$ we again find a finite solution for the Taylor approximation, but here with a constant offset and oscillation for all times. Thereby the amplitudes of the oscillations depend on the frequency and can be calculated using the Fourier transform of the solution of the schematic model in equilibrium.

We compare this Taylor approximation with the full schematic model and find that it fits well for some intermediate times, but after that the full solution decays to zero, a feat that we see in the Taylor approximation only directly at the glass transition. We analyze the decay of the full model to find the timescale that governs the decay.

The Taylor approximation can be used to derive a formula for the shear stress, including the first higher harmonic. We find that the first higher harmonic is given as the Fourier transform of the equilibrium solution multiplied with an oscillatory term of our approximation, evaluated at 2ω. We compare numerical results of this formula with experimental data for the limit of vanishing shear amplitude.

Contents

1. Introduction

Soft matter – easy to identify in everyday life as everything that is soft and squishy – can be characterized scientifically as matter where the bonds in the material are about as strong as the forces deforming it. So for us, things we can deform by hand are soft, because the matter consists of pieces that we can "melt apart" by the force applied by our hands [26].

This definition directly leads to the question how soft matter responds to deformation such as stretching or shearing. As soft matter is so relevant in our daily lives – everything from toothpaste, paint and ketchup to creams, lotions and most parts of our body is soft matter – lots of experiments have been done to understand and modify soft matter properties.

It has been found that for understanding its response to deformation it suffices to look not at the atomic level, but at length-scales of nano- to micrometers, because the structures at these scales have rather weak bonds, so deformation affects those rather than the underlying atomic ones. Even more, these structures can form different phases known from atomic matter, like liquid or amorphous or crystalline solid, but the effective temperature ranges are, as claimed above, accessible by deformation with "human sized" forces. Matter with such structures is called colloid. Usually, the term implies also that the structure is made of solid bodies of size of nano- to micrometers in a liquid. Often only the colloidal structure is needed to understand deformation phenomena, so the behavior of the system can be characterized by only a few parameters, like the temperature, the diameter of the particles, the number density and how they interact. Also, the liquids interaction with the particles can be simplified as Brownian motion of spheres, which are randomly being pushed by the molecules in the liquid, thus ignoring hydrodynamic interactions.

Nevertheless, colloidal systems show very diverse behavior: If the particles are elongated, they can form a nematic phase, where they all order parallel, but without any crystalline order. This is used for electric displays under the name liquid crystal display, or LCD. If the particles are long and stringy, like in ketchup or a polymer, the colloids history matters a lot for the systems dynamic properties, because the strings can be all jumbled up or in order. That's why ketchup comes easier out of the bottle when you shake it, thereby ordering the strings.

But even if the particles are round, hard spheres that do not interact with each other except by excluding volume, and move by Brownian motion, the system still shows complex behavior.

Depending on the size of the particles, the temperature (which makes the molecules of the liquid faster and so the Brownian motion stronger), and the volume density

of the hard spheres, the system can form a gas, a liquid or a crystalline solid. An example for a colloidal crystal are opals, where the colors come from colloidal crystals made of small spheres of silica [23]. However, even more things can happen. For example, in a fast cooling process (by temperature or by density changes) from a liquid or gas towards the solid, the particles may get stuck in a noncrystalline order and form an amorphous solid, a glass. For mixtures of two sizes of spheres this often is the standard behavior. The parameters of the glass transition are not identical with the crystal-liquid phase transition. It is also not clear whether this transition from liquid to glass is a phase transition in the classical sense where the thermodynamic partition function is smooth or not. Glasses can also be found on an atomic scale, for example metallic glasses. But as colloidal glass-forming particles are easier to observe experimentally (a microscope suffices), colloidal glasses are often studied to understand the glass transition in principle.

The glass transition is also called a dynamic transition, because the static structure factor (the Fourier transform of the particles' position at a certain time) shows no change at the transition, but the movement of particles over time changes: Experimentally, the particles stay very long in their place because the neighboring particles cage them, and for very long times, the power laws in how far they move are different from liquids. As the particles cannot move, the viscosity of the bulk material is very high. Because of this, the experimental definition of an atomic glass is an amorphous structure with a viscosity of 10^{12}poise or above [15].

There are not many theories that can predict the glass transition and some of its properties, and the existing theories often only work for atomic or for colloidal glasses. How the apparent mechanisms of glass-formation can be so different, but lead to similar overall behavior is still an open question.

One widely used theory for colloidal glasses and liquids is Mode Coupling Theory (MCT), created in 1984 by Bengtzelius, Götze and Sjölander [2] and studied in detail by Götze [14]. It defines the glass transition as a lengthening of dynamics so that the particles' coordinates stay correlated to their starting points, even for infinitely long times. That is mathematically expressed by the fact, that for long times the density correlator $\Phi(t)$ reaches a plateau value, instead of decaying to zero. Or, put differently, the longest relaxation time of the system diverges. Although the state-point predicted for the glass transition is slightly different from the one observed experimentally, and in experiments the correlation drops to zero for very long times, the predictions for a lot of properties are very good, and extensions of the original theory to multi-component [25, 17, 31], confined [24], sheared [11, 32, 22], active [13, 20] or granular [21] systems continue to give good results.

As explained above, one of the main properties of a glass, its reaction to shear, is an important aspect of soft matter that up to now difficult to grasp within MCT. For small shear linear perturbation theory has been studied, where it is possible to use the equilibrium equations [25]. For large shear, extensions have been made [11, 12, 3], which, however, remain difficult to implement numerically. Because of this, schematic models (simple toy models) of MCT are used that are hoped to

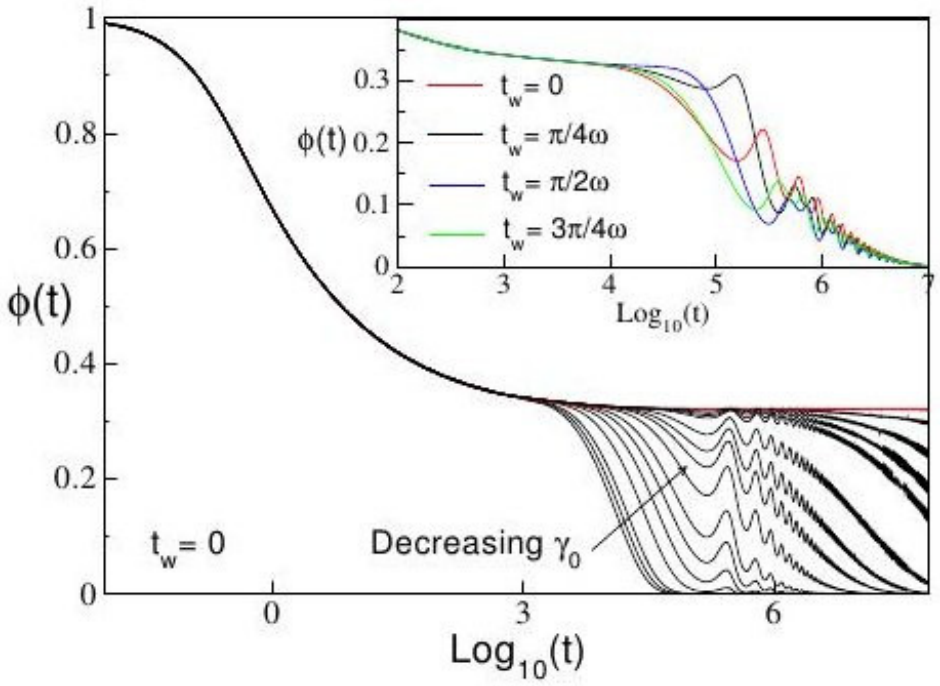

Figure 1.0.1.: For any nonzero stationary shear flow the correlator $\Phi(t-t',t')$ seems to decay to zero for long times t (for fixed $t' = t_w$), but with a diverging timescale. Parameters: $\omega = 2 \cdot 10^{-5}$, $\epsilon = 0.001$, figure unpublished by Joe Brader

capture the qualitative behavior of the systems while being easier accessible. A disadvantage of these models is that they need phenomenological parameters, while MCT is a true microscopic theory.

Several kinds of shear have been studied with schematic models, where they show good qualitative agreements with experiments [9, 29, 1]. Schematic MCT results for periodic shear were studied extensively by Brader et al. [4] and compared to simulation as well as experimental data. For this, the parameters were fitted using equilibrium values only, and then the results were compared for large shear with good results.

Brader observed that the correlator $\Phi(t-t',t')$ decays to zero for long times t (with t' fixed), but with a diverging timescale for vanishing shearing amplitude, $\gamma \to 0$, see fig. 1.0.1. This has also been found for linear shear, where the decay is always at about the same rescaled time $\dot{\gamma}t$ [18], that is, at the same shear strain. But for oscillatory shear, rescaling with the equivalent value $\omega\gamma_0 t$ does not give a master curve, and the strain does not increase over time.

However, if even for infinitely small oscillatory shear the correlator decays for long times, small disturbances of an experimental system would destroy the theoretically predicted ideal glass transition. This might mean that the liquid-glass transition

could just be masked in real life by all the small disturbances of the system, which would make the correlators in experiments drop to zero for large times.

Thus, to learn more about the nature of the glass transition, it is interesting to look a bit deeper into periodic shearing with vanishing amplitude to see how nonzero shear affects the correlator.

In this thesis we will assume that the correlator converges smoothly towards the equilibrium correlator, i.e. that a Taylor series ansatz of the shearing amplitude γ holds, even for long times. For this, we will use the schematic MCT deployed by Brader so we are able to compare results, and because it is one of the simplest models to yield nonzero higher harmonics. Higher harmonics – when the shear stress responds not with a perfect sine to a sinusoidal shear strain – cannot be calculated by linear perturbation theory from equilibrium, but it can be measured in experiments. A similar derivation has been done for the response to an electric field by Tarzia et al. [28].

The structure of this thesis is as follows:

In the first chapter the fundamentals needed for the analytical part of the thesis will be introduced. This includes the Mode Coupling Theory (MCT), a schematic MCT in equilibrium and under shear for parameters close to the glass transition.

A Taylor expansion of the schematic MCT used by Brader for small sinusoidal shear amplitudes will be derived in the second chapter. This gives equations for the first order perturbations of the correlator, which will be analyzed for long timescales, showing that the correlator expressions have oscillatory solutions.

The third chapter will compare numerical solutions of the Taylor expansion formulas with the analytical derivations, thus supporting the analytical results. Also, a comparison to the full model is made, where we find that the Taylor series approach works for intermediate time intervals.

In the fourth chapter, the analytical results will be used to derive the first order perturbation of the shear stress, including the first higher harmonic. We also present a short comparison of the third harmonic with experimental results.

A short conclusion wraps up the findings.

Additional information to mathematical formulas used and the numerical calculations is given in an appendix, as well as some additional figures.

2. Theoretical foundations

2.1. Mode Coupling Theory

The Mode Coupling Theory (MCT) describes liquids and colloidal glasses close to the glass transition. It was created in 1984 by Bengtzelius, Götze and Sjölander [2] for systems in equilibrium and has since been extended to sheared, driven, multi-component and many other systems where it has been successfully compared to experimental findings. [14]

2.1.1. MCT in Equilibrium

Here the central formulas of MCT and their derivation for an isotropic mono-disperse system with spherically symmetric colloidal particles, where the particles perform Brownian motion, are briefly presented. [7, 8, 27]

A microscopic analysis of the movements of N Brownian particles in terms of the Fourier transformed distribution function $n_k(t)$ (with $k = \left|\vec{k}\right|$because of isotropy)

$$n_k(t) = \sum_{i=1}^{N} e^{i\vec{k}\vec{r}_i(t)}$$

yields the Smoluchowski equation

$$\partial_t n_k(t) = \Omega^\dagger n_k(t)$$

with the adjoint Smoluchowski operator

$$\Omega^\dagger = \sum_{i=1}^{N} (\vec{\partial}_i + \vec{F}_i) \cdot \vec{\partial}_i,$$

where $\vec{F}_i = -\partial_i \mathcal{U}(\{\vec{r}_i\})$ is the internal force on one particle for the total interaction potential $\mathcal{U}$.

A central quantity for describing glassy phenomena is the density correlation function

$$\Phi_k(t) = \left\langle \frac{1}{N} n_k^*(t) n_k(0) \right\rangle_{TL},$$

where $\langle \dots \rangle_{TL}$ means averaging in the thermodynamic limit. Φ has as limits the static structure factor $S_k = \Phi_k(0)$ and the nonergodicity parameter

$$F_k = \Phi_k(t \to \infty).$$

F_k is zero if the system is ergodic, this means that a particles position after a long time is not affected by its starting point. If F_k is nonzero, a particle "remembers" even for infinitely long times where it has been, for example because is caged by its surrounding particles.

By projecting the time-evolution solution of the Smoluchowski equation

$$n_k(t) = e^{\Omega^\dagger t} n_k(0)$$

onto a reducible and an irreducible part, using the uniqueness of the solution of a differential equation and considering this in terms of the correlator $\Phi_k(t)$, we get a Zwanzig-Mori equation

$$\partial_t \Phi_k(t) + \Gamma_k(t)\{\Phi_k(t) + \int_0^t dt' m_k(t-t')\partial_{t'}\Phi_k(t')\} = 0. \tag{2.1.1}$$

$\Gamma_q(t) = D_0 q^2(t)/S_{q(t)}$ is the initial decay rate. This formula is exact, but it can only be evaluated with an approximation of the memory function m, which is a four-point correlation function.

Mode Coupling Theory approximates the memory function m as a product of two-point correlation functions. This yields

$$m_q(t) = \frac{1}{2N} \sum_k \frac{S_q S_k S_p}{q^4} V_{\vec{q}\vec{k}\vec{p}} V_{\vec{q}\vec{k}\vec{p}} \Phi_k(t) \Phi_p(t)$$

with the vertex functions

$$V_{\vec{q}\vec{k}\vec{p}} = \vec{q} \cdot (\vec{k} n c_k + \vec{p} n c_p) \delta_{\vec{q},\vec{k}+\vec{p}},$$

where the equation for $m_k(t)$ can be seen as a bilinear functional $\mathcal{F}$ of the correlation function Φ. The direct correlation function c_k is given by the Ornstein-Zernike relation

$$S_k = 1/(1 - n c_k).$$

By using the Zwanzig-Mori equation with the approximation for $m_k(t)$, we get a fix-point relation for F_k

$$F_k = S_k - \{S_k^{-1} + \mathcal{F}(F_k, F_k)\}^{-1}. \tag{2.1.2}$$

At the glass transition the system becomes non-ergodic, so there F jumps from zero to a nonzero value. The fix-point relation has a bifurcation at this point, so in a glass the equation has two solutions, zero and a nonzero value. Therefore it is possible to calculate the parameters of the glass transition with MCT equations, using the static structure factor S as input.

2.1.2. MCT with shear

Under shear, the system is no longer isotropic, and the adjoint Smoluchowski operator is [4]

$$\Omega^\dagger(t) = \sum_i D_0[\partial_i + \beta \mathbf{F}_i] \cdot \partial_i + D_0 \dot{\gamma}(t) y_i \frac{\partial}{\partial x},$$

with $\beta = \frac{1}{k_B T}$, temperature T and D_0 as short-time diffusion coefficient at infinite dilution.

The dependence of the shear stress $\sigma(t)$ on the shear strain rate $\dot{\gamma}(t')$ can be given by a generalized Green-Kubo relation

$$\sigma(t) = \int_{-\infty}^{t} dt' \dot{\gamma}(t') G(t, t'), \tag{2.1.3}$$

where $G(t, t')$ is the shear modulus (which also depends on the shear strain rate)

$$G(t, t') = \frac{1}{k_B T V} \left\langle \hat{\sigma}_{xy} \exp_-(\int_{t'}^{t} ds \Omega^\dagger(s)) \hat{\sigma}_{xy} \right\rangle$$

with system volume V, a time-ordered exponential function because $\Omega^\dagger$ does not commute for different times and a fluctuating stress tensor element $\hat{\sigma}_{xy} = -\sum_i F_i^x y_i$.

We can split the shear stress into its Fourier modes $G_n(\omega) = G'_n(\omega) + iG''_n(\omega)$ with (for periodic strain of frequency ω)

$$\sigma(t) = \gamma_0 \sum_{n=1}^{\infty} G'_n(\omega) \sin(n\omega t) + \gamma_0 \sum_{n=1}^{\infty} G''_n(\omega) \cos(n\omega t) \tag{2.1.4}$$

$$= \gamma_0 \frac{1}{2i} \sum_{n=1}^{\infty} G_n(\omega) e^{in\omega t} + c.c. \tag{2.1.5}$$

$$G'_n(\omega) = \frac{\omega}{\pi} \int_{-\pi/\omega}^{\pi/\omega} dt\, \sigma(t) \sin(n\omega t) \tag{2.1.6}$$

$$G''_n(\omega) = \frac{\omega}{\pi} \int_{-\pi/\omega}^{\pi/\omega} dt\, \sigma(t) \cos(n\omega t) \tag{2.1.7}$$

We can also split the complex modulus into amplitude $I_n = |G_n|$ and phase shift $\delta_n = \arctan(G''_n/G'_n)$. For small strain, one might assume a linear response regime with $I_n = 0\ \forall n \neq 1$.

2.2. The schematic model

Calculating the MCT equations for equilibrium is already cumbersome, and under shear the equations have a full $\vec{k}$-dependence and additional terms. Therefore it is

more convenient to switch to a schematic model that is easier to calculate but might still show the qualitative features of the full model.

In a schematic model, the MCT equations are used, but simplified for one wave vector only, $m_{\vec{k}}(t) \to m(t)$. This is justified by the experience that the results of full MCT for the different wave vectors are similar [6]. The complicated formula for the vertex $m(t)$ is replaced by a simple polynomial ansatz (in this case second order), where the coefficients are phenomenological parameters that need to be determined empirically by comparison to experiments and are chosen to study the glass transition.

2.2.1. Equilibrium equation

As we will later use the equilibrium solution as input for the sheared Taylor approximation, a closer look is necessary. In equilibrium, the correlator $\Phi_{eq}(t)$ satisfies [14]:

$$0 = \dot{\Phi}_{eq}(t) + \Phi_{eq}(t) + \int_0^t ds\, m_{eq}(t-s)\dot{\Phi}_{eq}(s) \tag{2.2.1}$$

$$m_{eq}(t) = v_1\Phi_{eq}(t) + v_2\Phi_{eq}^2(t) \tag{2.2.2}$$

$$\Phi_{eq}(0) = 1 \tag{2.2.3}$$

The relation of the equilibrium schematic model to full MCT in equilibrium is directly visible in comparison to equation (2.1.1), with $S_k \to 1$. We set $\Gamma = 1$, which leads to a rescaling in time and frequency: $t_{\text{rescaled}} = t/\Gamma$ and $\omega_{\text{rescaled}} = \Gamma \cdot \omega$. The parameters v_1 and v_2 from the polynomial ansatz can be varied freely, but as we want to look at the glass transition, we set $v_2 = 2$ and $v_1 = 2(\sqrt{2}-1)+\epsilon(\sqrt{2}-1)^{-1}$, where ϵ is the distance to the glass transition; for $\epsilon < 0$ we have a liquid and otherwise a glass. In fig. 2.2.1 some solutions for different values of ϵ are plotted. The decay from the initial value 1 to a first plateau value is called β-decay. In a liquid, the solution decays further to zero (α-decay). The timescale of the α-decay increases towards infinity for $\epsilon \to 0$.

Long-time limit The long-time limit of the correlator can be calculated via the Laplace transform $F(p)$ as $pF(p) \overset{p\to 0}{\longrightarrow} f(t \to \infty)$, see appendix A.2 for a definition. This gives a formula similar to the one presented in eq. (2.1.2) for the full MCT:

$$m_{eq}^{\infty} = \frac{f_{eq}^{\infty}}{1 - f_{eq}^{\infty}} \tag{2.2.4}$$

Fourier transform It is common to study the Fourier transform in terms of the function $\chi(\omega) = \chi'(\omega) + i\chi''(\omega)$

$$\chi(\omega) = i\omega LT\{\Phi_{eq}\}(i\omega) = i\omega FT\{\Phi_{eq}\}(\omega) = \overline{\chi}(-\omega) \tag{2.2.5}$$

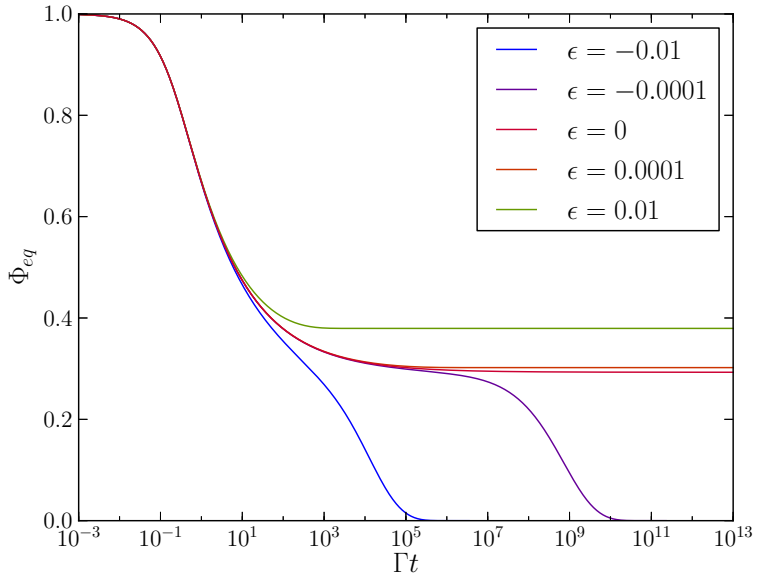

Figure 2.2.1.: Schematic MCT in equilibrium: The correlator $\Phi_{eq}(t)$ develops a plateau value f_{eq}^{∞} for long times in the glass, $\epsilon \geq 0$, and decays to zero in the liquid, $\epsilon < 0$.

In fig. 2.2.2 some typical curves are shown, for a detailed treatment see [16]. The numerical algorithm used to evaluate the Fourier transform is described in appendix B.1. The correlators are calculated using the methods explained in appendix B.2 and checked using two different programs, one by David Hajnal and one self written. The equilibrium correlators will be used as input for the Fourier transform of the evaluated formulas in chapter 3 for the visualization of the results and in chapter 4 as input for the numerical calculation of the Taylor approximation.

As it will be important later on, let us take a closer look at one specific feature in the plot of $\chi''(\omega)$, fig. 2.2.2. For $\epsilon < 0$, $\chi''(\omega)$ is proportional to ω^a, $a < 1$, for some intermediate range of ω, but for small ω goes proportionally toω^{-b} towards a second maximum (α-relaxation, corresponding to the decay of the correlator $\Phi_{eq}(t)$ from the plateau to equilibrium). For $\epsilon = 0$, $\chi''(\omega)$ is proportional to ω^a, $a < 1$, for all values of ω after the maximum at $\omega \approx 1$ (α-relaxation takes infinitely long in the glass, therefore the maximum of the liquid is shifted to infinitely small ω). For $\epsilon > 0$, $\chi''(\omega)$ is proportional to ω^a for some intermediate range of ω, but for small ω, it grows proportionally to ω. So the Fourier transform itself is constant there. The value of ω at which this occurs seems to be proportional to the power of ϵ. In the analytical chapter, this linear region will lead to constant plateaus of some long-time limits we will analyze.

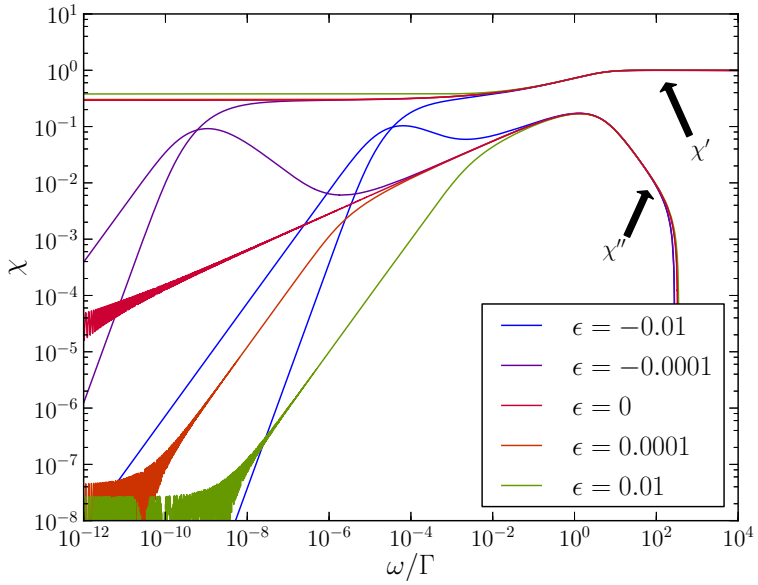

Figure 2.2.2.: Schematic MCT in equilibrium: $\chi(\omega) = \chi'(\omega) + i\chi''(\omega)$ in the glass, $\epsilon \geq 0$, and in the liquid, $\epsilon < 0$.

2.2.2. Equation with shear and TTI

A simple way to extend the schematic MCT to sheared systems [10] is by introducing a shear dependent term into the memory function:

$$\begin{aligned} 0 &= \frac{1}{\Gamma}\dot{\Phi}(t) + \Phi(t) + \int_0^t ds\, m(t-s)\dot{\Phi}(s) \\ m(t) &= h(t)\left[v_1\Phi(t) + v_2\Phi^2(t)\right] \\ h(t) &= \Big[1 + (\gamma_0\omega t)\Big]^{-1} \end{aligned}$$

The shear modulus can be defined as $G(t,t') = v_\sigma\Phi^2(t-t')$. The model was used to study linear shear, with $h(t) = \Big[1 + (\dot{\gamma}t)\Big]^{-1}$. However, it is easy to show that this model yields no higher harmonics for oscillatory shear, $I_n = 0\ \forall n > 1$, because of its time-translational invariance (TTI). Also, the proposed Taylor ansatz will not work with this model, because we always have terms $\gamma \cdot t$, so $\gamma \to 0$ is well defined only for finite time intervals, but we want to study the long-time limit as well.

2.2.3. Equation with shear

A more complicated schematic MCT model for arbitrary shear $F_{12}^{\dot{\gamma}}$ [5] that has been studied intensively is

$$0 = \frac{1}{\Gamma}\dot{\Phi}(t,t') + \Phi(t,t') + \int_{t'}^{t} ds\, m(t,s,t')\dot{\Phi}(s,t') \qquad ,t' \leq t \tag{2.2.6}$$

$$m(t,s,t') = h(t,t')h(t,s)\left[v_1\Phi(t,s) + v_2\Phi^2(t,s)\right] \tag{2.2.7}$$

$$h(t,t') = \left[1 + \frac{1}{\gamma_c^2}\int_{t'}^{t} ds\,\dot{\gamma}(s)\right]^{-1} \tag{2.2.8}$$

$$= \left[1 + \left(\frac{\gamma_0}{\gamma_c}\right)^2 \left(\sin\omega t - \sin\omega t'\right)^2\right]^{-1} \qquad (\text{for } \gamma(t) = \gamma_0 \sin\omega t). \tag{2.2.9}$$

The initial condition is $\Phi(t,t) = 1$. We will use rescaled parameters by setting $\Gamma = 1$. To get non-rescaled parameters, set $t_{\text{new}} = {}^{t_{\text{rescaled}}}/_{\Gamma}$ and $\omega_{\text{new}} = \Gamma \cdot \omega_{\text{rescaled}}$. We will also use $\gamma = \frac{\gamma_0}{\gamma_c}$ as abbreviation. For this schematic model, the shear modulus can be defined as

$$G(t,t') = v_\sigma \Phi^2(t,t'). \tag{2.2.10}$$

Different to the model before, we have two time variables and, for oscillatory shear, no time-translational invariance (can be seen from the form of $h(t,t')$). As for the equilibrium model, we will use $v_2 = 2$ and $v_1 = 2(\sqrt{2}-1) + \epsilon(\sqrt{2}-1)^{-1}$, so that for $\epsilon < 0$ we have a liquid and otherwise a glass. For oscillatory shear we have $\Phi(t,t') = \Phi(t + \frac{\pi}{\omega}, t' + \frac{\pi}{\omega})$, because the only explicit occurrence of t and t' is in $h(t,t')$, which is periodic, and the periodicity also fits our initial condition. So one only needs to consider the time interval $t \in [0, \frac{\pi}{\omega}]$.
With these equations it is possible to numerically calculate $\Phi(t,t')$. This has been done by Brader et al. [4]. However, for $\gamma = \frac{\gamma_0}{\gamma_c} \to 0$ the relaxation time diverges (see fig. 1.0.1), leading to ever more time consuming calculations.

Because of this, in this thesis we will look at the first term of a Taylor expansion of the original equations for small amplitude of the shear $\gamma \to 0$ to come to a simplified expression and examine the behavior of the first higher harmonic amplitude $\frac{I_3}{I_1}$ in that limit.

3. Analytical results

This chapter will be very mathematical, so let us start with a short summary of the main results.

We will insert a Taylor ansatz of second order into the schematic model for oscillatory shear that was introduced in subsection 2.2.3. The zeroth order of this equations gives the equilibrium equation. We therefore consider the second order equation, transforming it to two linear integro-differential equations. Their two solutions, $f_0(t-t')$ and $f_1(t-t')$, are the first two Fourier coefficients of a Fourier series with respect to $t+t'$ that form the second order Taylor approximation of the equilibrium solution.

We continue with analyzing the long-time limit behavior of f_0 and f_1. As mentioned in the introduction, the full solutions seem to decay to zero for all $\gamma > 0$, but with a diverging timescale for $\gamma \to 0$. We also know that if a Taylor series exists and converges to the right values, the approximations usually converge point-wise and are bounded on every compact set. So we expect the solutions to behave in one of two ways:

- We could expect some simple bounded function, for example constant or oscillatory. This would mean that for every γ there is a time t, where the Taylor approximation is not good any more, because there the decay starts, and that is not described by the Taylor approximation. But as that time diverges for $\gamma \to 0$, we still would get a point-wise approximation. If this is the case, however, we learn nothing about the decay from analyzing the approximation.
- The other possibility is that the Taylor approximation diverges. Then the values would still be bounded for every finite time t, but by analyzing the approximation, we could learn something about the decay. The divergence of the approximation might be difficult to show analytically, but this is the outcome we might wish for, as understanding the decay is one of the main reasons for the analysis.

To find out which of these two possibilities is the case, we will analyze the long-time behavior of the two equations for f_0 and f_1 using Laplace transformation.

For the following presentation of the analytically calculable properties of the Taylor approximation a mainly mathematical view will be adopted, the physical implications will be considered later on. The casual reader may jump to the last section of the chapter, 3.4, where a comprehensive review of the results and the arising questions will be given, possibly after a quick look into section 3.2, where the final equations of the second order perturbation of the equilibrium solution are presented.

3.1. Derivation of the second order Taylor equations

We will use rescaled parameters for derivation and numerical calculation by setting $\Gamma = 1$. To get non-rescaled parameters, set $t_{\text{new}} = {}^{t_{\text{rescaled}}}/_{\Gamma}$ and $\omega_{\text{new}} = \Gamma \cdot \omega_{\text{rescaled}}$. We will also use $\gamma = \frac{\gamma_0}{\gamma_c}$ as abbreviation. With some minor transformations, our full set of schematic MCT equations (see also subsection 2.2.3) read

$$0 = \frac{d}{dt}\Phi(t,t') + \Phi(t,t') + h(t,t')\int_0^{t-t'} ds\, m_0(t,t'+s)\frac{d}{ds}\Phi(t'+s,t') \tag{3.1.1}$$

$$m_0(t,t') = h(t,t')\left[v_1\Phi(t,t') + v_2\Phi^2(t,t')\right] \tag{3.1.2}$$

$$h(t,t') = \left[1+\gamma^2 h_\omega(t,t')\right]^{-1} \tag{3.1.3}$$

$$h_\omega(t,t') = \left(1-\cos\omega(t-t')\right)\left(1+\cos\omega(t+t')\right), \tag{3.1.4}$$

with $v_2 = 2$ and $v_1 = 2(\sqrt{2}-1) + \epsilon(\sqrt{2}-1)^{-1}$.

3.1.1. Important steps of the derivation

We assume that a Taylor expansion of $h(t,t')$ and $\Phi(t,t')$ for small γ can be made, with the initial condition $\Phi_\omega(t,t) = 0$:

$$h(t,t') = 1 - \gamma^2 h_\omega(t,t') + O(\gamma^4) \tag{3.1.5}$$

$$\Phi(t,t') = \Phi_{eq}(t-t') + \gamma^2\Phi_\omega(t,t') + O(\gamma^4) \tag{3.1.6}$$

Due to symmetry, $\Phi(t,t')$ should only have even powers of γ, so the smallest is of quadratic order. This can also be checked using the ansatz $\Phi(t,t') = \Phi_{eq}(t-t') + \gamma^a\Phi_a(t,t') + \gamma^2\Phi_\omega(t,t') + O(\gamma^4)$, with $0 < a < 2$. Because the only inhomogeneity comes from $h(t,t')$, this gives $\Phi_a(t,t') = 0$.

Inserting this ansatz into eq. (3.1.1) and assuming all the integrals converge gives us an equation with even orders of γ. We will ignore all terms higher than second order.

The zeroth order equation yields the equilibrium equation (2.2.1) for $\Phi_{eq}(t)$. As $\Phi_{eq}(t)$ fulfills the equation by definition, this is zero and we are left with only the second order terms. Multiplying with γ^{-2} and integration by parts gives a linear

integro-differential equation:

$$\begin{aligned}0 = &\frac{d}{dt}\Phi_\omega(t,t') + (1+v_1+v_2)\Phi_\omega(t,t') \\ &+ \int_0^{t-t'} ds\left[v_1 + 2v_2\Phi_{eq}(t-t'-s)\right]\Phi_\omega(t,t'+s)\dot{\Phi}_{eq}(s) \\ &+ \int_0^{t-t'} ds\left[v_1 + 2v_2\Phi_{eq}(s)\right]\Phi_\omega(t-s,t')\dot{\Phi}_{eq}(s) \\ &+ h_\omega(t,t')(\dot{\Phi}_{eq}(t) + \Phi_{eq}(t)) - \int_0^{t-t'} ds\, h_\omega(t,t'+s)m_{eq}(t-t'-s)\dot{\Phi}_{eq}(s).\end{aligned} \tag{3.1.7}$$

With a transformation of variables $v = t - t', u = t + t'$ with $\Phi_\omega(t,t') = \tilde{\Phi}(v,u)$, see fig. 3.1.1, we get

$$\begin{aligned}0 = &\partial_v\tilde{\Phi}(v,u) + \partial_u\tilde{\Phi}(v,u) + (1+v_1+v_2)\tilde{\Phi}(v,u) \\ &+ \int_0^{v} ds\,\Phi'_{eq}(s)\left[v_1 + 2v_2\Phi_{eq}(s)\right]\cdot\tilde{\Phi}(v-s,u-s) \\ &+ \int_0^{v} ds\,\Phi'_{eq}(s)\left[v_1 + 2v_2\Phi_{eq}(v-s)\right]\cdot\tilde{\Phi}(v-s,u+s) \\ &+ \tilde{h}_\omega(v,u)(\dot{\Phi}_{eq}(v) + \Phi_{eq}(v)) - \int_0^{v} ds\,\Phi'_{eq}(s)\cdot m_{eq}(v-s)\tilde{h}_\omega(v-s,u+s).\end{aligned} \tag{3.1.8}$$

Now, using the periodicity $\Phi(t,t') = \Phi(t+\frac{\pi}{\omega}, t'+\frac{\pi}{\omega})$, or $\tilde{\Phi}(v,u) = \tilde{\Phi}(v,u+\frac{2\pi}{\omega})$, we use a Fourier series in u

$$\tilde{\Phi}(v,u) = \sum_{n=-\infty}^{\infty} e^{in\omega u} f_n(v). \tag{3.1.9}$$

With this we find that for $n \notin \{0, \pm 1\}$ the solutions are zero, because the inhomogeneity is zero. We also know that $f_{-1}(v) = cc\{f_1(v)\}$. The equations for the two still necessary nonzero Fourier modes f_0 and f_1 are our final equations, together with the Fourier sum to stick them together again.

3.2. Schematic model in quadratic order

Here the results of the derivation are summarized. The solution of the Taylor approximation is

$$\Phi(t,t') = \Phi_{eq}(t-t') + \gamma^2\Phi_\omega(t,t') + O\left(\gamma^4\right) \tag{3.2.1}$$

$$\begin{aligned}\Phi_\omega(t,t) &= f_0(t-t') + e^{i\omega(t+t')}f_1(t-t') + e^{-i\omega(t+t')}cc\{f_1(t-t')\} \\ &= f_0(t-t') + 2\cos(\omega(t+t'))f_R(t-t') + 2\sin(\omega(t+t'))f_I(t-t')\end{aligned}$$

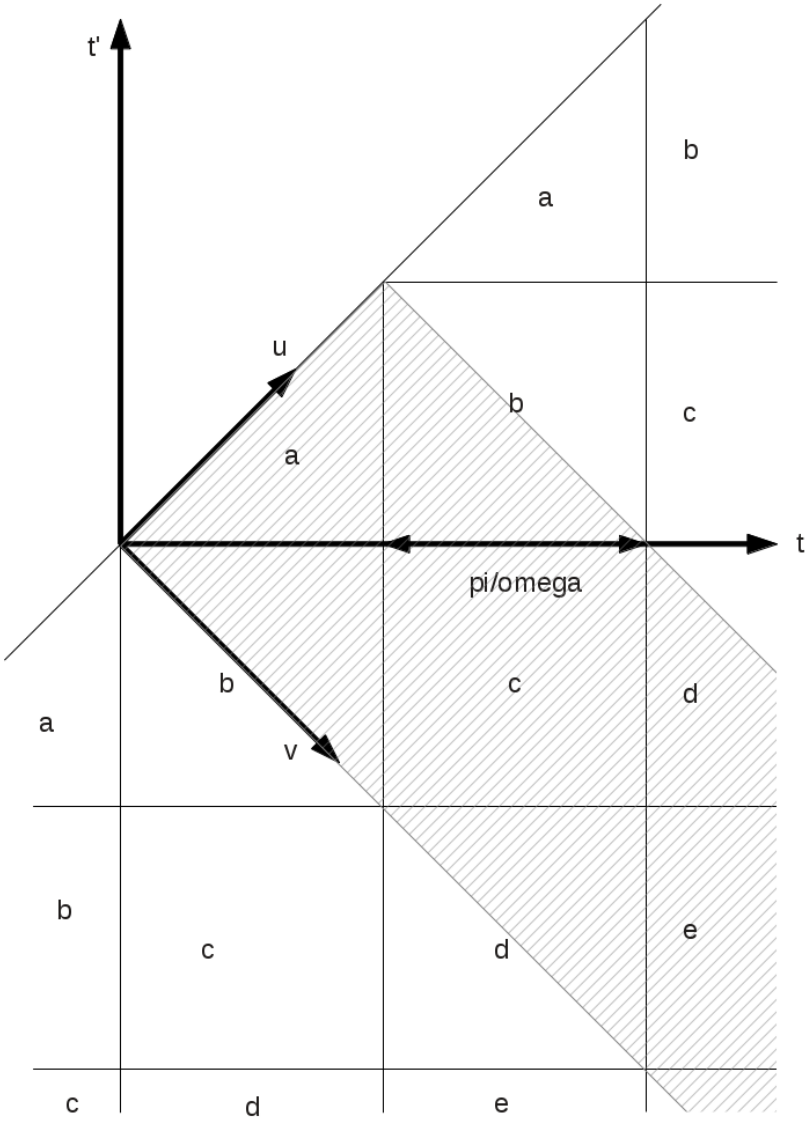

Figure 3.1.1.: Symmetries in time-space of the correlator (square with same number means that the correlator is the same for these parts). Axes for t, t', u and v are given. The part of the space that needs to be calculated is marked in gray stripes.

This formula is equivalent to one found by Tarzia et al. [28] for dielectric susceptibility. The two functions f_0 and $f_1 = f_R + if_I$ are given by linear integro-differential equations with the equilibrium correlator as input.

The equation for $f_0(v) \in \mathbb{R}$ with the initial condition $f_0(0) = 0$ is

$$\begin{aligned} 0 = {} & f_0'(v) + (1 + v_1 + v_2)\, f_0(v) \\ & + 2\int_0^v ds f_0(v-s)\Phi_{eq}'(s)\left[v_1 + v_2\Phi_{eq}(v-s) + v_2\Phi_{eq}(s)\right] \\ & + (2 - \cos\omega v)(\Phi_{eq}'(v) + \Phi_{eq}(v)) \\ & + \int_0^v ds \Phi_{eq}'(s)\cdot m_{eq}(v-s)\cos\omega(v-s). \end{aligned} \tag{3.2.2}$$

For the equation for $f_1(v) = f_R(v) + if_I(v)$ with initial condition $f_1(0) = 0$ we get

$$\begin{aligned} 0 = {} & f_1'(v) + (1 + v_1 + v_2 + i\omega)\, f_1(v) \\ & + 2\int_0^v ds f_1(v-s)\Phi_{eq}'(s)\left[v_1\cos\omega s + v_2 e^{i\omega s}\Phi_{eq}(v-s) + v_2 e^{-i\omega s}\Phi_{eq}(s)\right] \\ & + \frac{1}{2}(1 - \cos\omega v)\left[\Phi_{eq}'(v) + \Phi_{eq}(v)\right] \\ & - \frac{1}{2}\int_0^v ds\, e^{i\omega s}\Phi_{eq}'(s)\cdot m_{eq}(v-s)\left[1 - \cos\omega(v-s)\right]. \end{aligned} \tag{3.2.3}$$

The remainder of the chapter will be spent analyzing the long-time behavior of the solutions f_0 and f_1. We will consider Φ_ω only in the next chapter, comparing it to the full solution.

3.3. Long-time limit

In this section we study the long-time limit of the correlator $\Phi(t, t')$ by doing a Laplace transformation (see appendix A.2 for the definition) of the integro-differential equations describing f_0 and f_1, eq. (3.2.2) and (3.2.3). For this, we assume the convergence of the transformation and the existence of the long-time limits.

Since we already know that $\Phi_{eq}(t)$ converges to zero for $\epsilon < 0$, we are only interested in the case $\epsilon \geq 0$. For $\epsilon < 0$, the long-time limits are simply zero.

3.3.1. Long-time limit of $f_0(v)$

We shorten the expressions by defining $LT\{f_0(t)\}(p) = F_0(p)$, $LT\{\Phi_{eq}(t)\}(p) = F_{eq}(p)$ and $LT\{\Phi^2_{eq}(t)\}(p) = F_{2eq}(p)$. A Laplace transform of eq. (3.2.2) yields:

$$\begin{aligned}
F_0(p) \cdot &\left[p + v_2 LT\{\frac{d}{dv}\Phi^2_{eq}(v)\}(p) + 2v_1(pF_{eq}(p) - 1)\right] \\
&+ LT\{\Phi_{eq}(v) f_0(v)\}(p) \cdot 2v_2\,(pF_{eq}(p) - 1) \\
= &- 2\,(pF_{eq}(p) - 1 + F_{eq}(p)) \\
&+ \frac{1}{2} LT\{\dot{\Phi}_{eq}(v) + \Phi_{eq}(v)\}(p - i\omega) - \frac{1}{2}(pF_{eq}(p) - 1) LT\{m_{eq}(v)\}(p - i\omega) \\
&+ \frac{1}{2} LT\{\dot{\Phi}_{eq}(v) + \Phi_{eq}(v)\}(p + i\omega) - \frac{1}{2}(pF_{eq}(p) - 1) LT\{m_{eq}(v)\}(p + i\omega)
\end{aligned}$$

We have used $2f'(t)f(t) = \frac{d}{dt}f^2(t)$ to simplify the equation. Expressing the cosine as exponential functions leads to the frequency shifts, see appendix A.2. Our previous discussion of $\Phi_{eq}(t)$ in section 2.2.1 helps us understand the behavior of the right-hand side: For $\epsilon \geq 0$, $F_{eq}(p)$ has a pole at $p = 0$ and is finite everywhere else, the right-hand side diverges for $p = 0, \pm i\omega$ and is finite otherwise. This lets us make as ansatz for f_0

$$\begin{aligned}
f_0(v) &= g_0(v) + f_0^\infty + f_0^\omega e^{i\omega v} + \bar{f_0^\omega} e^{-i\omega v} \\
F_0(p) &= G_0(p) + \frac{f_0^\infty}{p} + \frac{f_0^\omega}{p - i\omega} + \frac{\bar{f_0^\omega}}{p + i\omega}
\end{aligned} \tag{3.3.1}$$

with $\lim_{v\to\infty} g_0(v) = 0$ and, since $f_0(v)$ is real, $\bar{f_0^\omega} e^{-i\omega v}$ instead of $f_0^{-\omega} e^{-i\omega v}$. We get

$$\begin{aligned}
f_0^\infty &= \frac{-2f_{eq}^\infty}{1 - v_1 + 2(v_1 - v_2)f_{eq}^\infty + 3v_2(f_{eq}^\infty)^2} \\
f_0^\omega &= \frac{\frac{1}{2}m_{eq}^\infty[2 - f_{eq}^\infty - \chi(\omega)]}{1 - v_1 + i\omega - 2v_2 f_{eq}^\infty + 2(v_1 + v_2 f_{eq}^\infty)\chi(\omega) + v_2\chi_2(\omega)}
\end{aligned} \tag{3.3.2}$$

Here we use $\chi(\omega) = i\omega F_{eq}(i\omega)$ and $\chi_2(\omega) = i\omega F_{2eq}(i\omega)$. These results are also valid for $\epsilon < 0$: $f_{eq}^\infty = 0$, so the limits are zero. We can also rewrite

$$f_0(v) = g_0(v) + f_0^\infty + A_0 \cos(\omega v + \delta_0). \tag{3.3.3}$$

We can evaluate the formulas using $\chi(\omega)$ as shown in fig. 2.2.2, calculated numerically with the scheme given in chapter B. f_0^∞, plotted in fig. 3.3.1, is independent of frequency, and so given relative to ϵ. The colored dots mark the color of the matching lines with the same ϵ in the plot of A_0 and δ_0, which are given in dependence of ω and plotted in fig. 3.3.2. For $\epsilon \to 0$, the long-time limit f_0^∞ diverges with $\epsilon^{-1/2}$. This can be shown analytically: We have $f_{eq}^\infty \to a + b\sqrt{\epsilon}$ with $a = 1 - \frac{\sqrt{2}}{2}$,

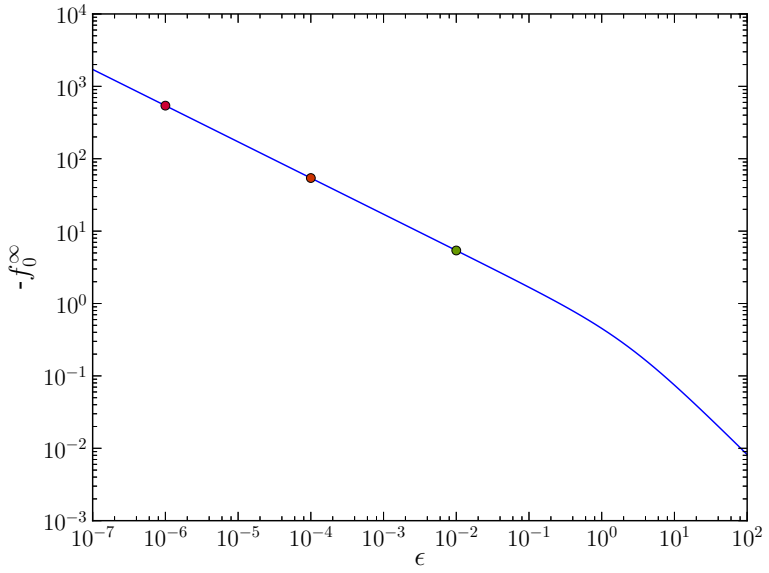

Figure 3.3.1.: The constant part $f_0^\infty(\epsilon)$ of the long-time limit of f_0 does not depend on ω and diverges for $\epsilon \to 0$ with $\epsilon^{-0.5}$. The dots mark the matching lines in the following figures.

$b = \frac{\sqrt{2+\sqrt{2}}}{2}$. Inserting this into the long-time limit of f_0^∞ yields

$$f_0^\infty \to \frac{-1}{\sqrt{2+\sqrt{2}}} \cdot \frac{1}{\sqrt{\epsilon}} \tag{3.3.4}$$

This seems to be a good approximation even for rather large ϵ, up to about $\epsilon = 1$.

Amplitude A_0 and phase shift δ_0 can be seen in fig. 3.3.2 for selected values of ϵ. Since A_0 depends on $\chi(\omega)$, the features are closely related to it. The most distinctive is the plateau for small ω, where the height depends on ϵ. For $\epsilon \to 0$ the value of the plateaus goes to infinity and starts at decreasing ω. The plateau corresponds to the regime $\chi(\omega) \propto \omega$ that was introduced in subsection 2.2.1. The dots on the left side of the figure are the analytical limits of the amplitude A_0 for $\omega \to 0$, see also subsection 3.3.3, supporting the assumption that the plateau is the real limit for $\omega \to 0$. For large ω ($\omega \approx 1$) we see a bend in the amplitude, right where χ has its maximum. For large ω, the amplitude goes to zero. However, the model simplifies the short time behavior, so the results for large ω are generally unphysical. For values of ω larger than the plateau, the curves for $\epsilon > 0$ follow a common master curve formed by the plot for $\epsilon = 0$. This is also an effect found for $\chi(\omega)$.

The inset shows the phase shift δ_0. On the plateau, $f_0(v)$ is in phase with $\dot{\gamma}(t)$. For $\epsilon \to 0$, as the plateau disappears, it seems as if the phase shift is nonzero for low frequencies. However, numerical errors prevent a conclusive answer.

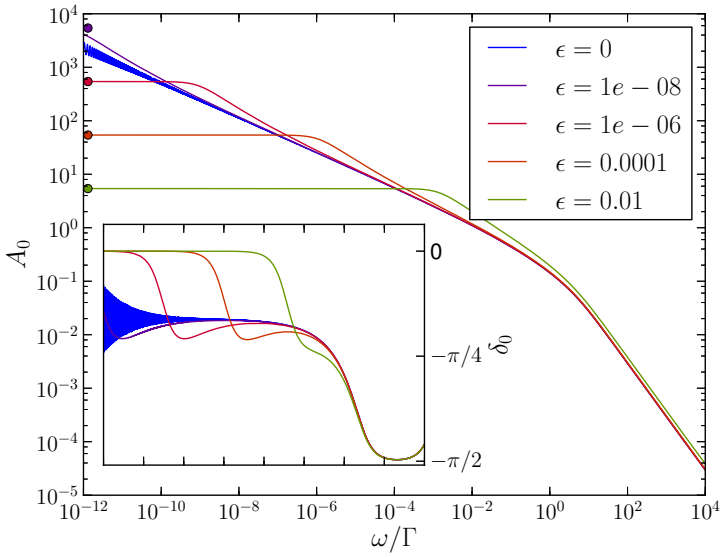

Figure 3.3.2.: Amplitude A_0 of the long-time oscillation of f_0. The dots mark the values at the limit $\omega \to 0$ for the selected values of ϵ. The inset shows the phase shift δ_0, plotted over the same frequency range as the amplitude.

3.3.2. Long-time limit of $f_1(v)$

The derivation of the long-time limit is analogous to that of $f_0(v)$.
A Laplace transform of (3.2.3) with $LT\{m_{eq}(t)\}(p) = M_{eq}(p)$ yields:

$$\begin{aligned}
&F_1(p)\left[p + 1 - v_1 + i\omega + (p + i\omega)M_{eq}(p + i\omega) + v_1(p - i\omega)F_{eq}(p - i\omega)\right] \\
&\quad + LT\{\Phi_{eq}(v)f_1(v)\}(p) \cdot 2v_2[(p - i\omega)F_{eq}(p - i\omega) - 1] \\
&= -\frac{1}{2}\left[pF_{eq}(p) - 1 + F_{eq}(p)\right] \\
&\quad + \frac{1}{2}\left[(p - i\omega)F_{eq}(p - i\omega) - 1 + F_{eq}(p - i\omega)\right] \\
&\quad + \frac{1}{4}\left[(p + i\omega)F_{eq}(p + i\omega) - 1 + F_{eq}(p + i\omega)\right] \\
&\quad - \frac{1}{4}\left[(p - i\omega)F_{eq}(p - i\omega) - 1\right]\left[M_{eq}(p + i\omega) - 2M_{eq}(p)\right]
\end{aligned}$$

We use as ansatz for f_1:

$$\begin{aligned}
f_1(v) &= g_1(v) + f_1^{\infty} + f_1^{\omega}e^{i\omega v} + f_1^{-\omega}e^{-i\omega v} \\
F_1(p) &= G_1(p) + \frac{f_1^{\infty}}{p} + \frac{f_1^{\omega}}{p - i\omega} + \frac{f_1^{-\omega}}{p + i\omega}
\end{aligned} \tag{3.3.5}$$

with $\lim_{v\to\infty} g_1(v) = 0$, and $f_1^{-\omega} \neq \bar{f_1^{\omega}}$ as $f_1(v)$ is complex. We get

$$\begin{aligned} f_1^{\infty} &= \frac{-\frac{1}{2}m_{eq}^{\infty}[2 - f_{eq}^{\infty} - \chi(-\omega)]}{1 - v_1 + i\omega - 2v_2 f_{eq}^{\infty} + v_1\chi(\omega) + (v_1 + 2v_2 f_{eq}^{\infty})\chi(-\omega) + v_2\chi_2(\omega)} \\ f_1^{\omega} &= \frac{\frac{1}{2}f_{eq}^{\infty}}{1 - v_1 + 2i\omega + (v_1 - 2v_2)f_{eq}^{\infty} + 2v_2(f_{eq}^{\infty})^2 + v_1\chi(2\omega) + v_2\chi_2(2\omega)} \\ f_1^{-\omega} &= \frac{\frac{1}{4}\left[f_{eq}^{\infty} + m_{eq}^{\infty}(1 - \chi(-2\omega))\right]}{1 - v_1 + m_{eq}^{\infty} - 2v_2 f_{eq}^{\infty} + (v_1 + 2v_2 f_{eq}^{\infty})\chi(-2\omega)} \end{aligned} \tag{3.3.6}$$

This can be split in real and imaginary part $f_1 = f_R + if_I$:

$$\begin{aligned} f_R(v) &= g_R(v) + f_R^{\infty} + f_R^{\omega}e^{i\omega v} + \bar{f_R^{\omega}}e^{-i\omega v} \\ f_I(v) &= g_I(v) + f_I^{\infty} + f_I^{\omega}e^{i\omega v} + \bar{f_I^{\omega}}e^{-i\omega v} \end{aligned}$$

with

$$f_R^{\omega} = \frac{1}{2}(f_1^{\omega} + \overline{f_1^{-\omega}}),\ f_I^{\omega} = \frac{1}{2i}(f_1^{\omega} - \overline{f_1^{-\omega}}).$$

As for f_0, we can rewrite f_R as

$$f_R(v) = g_R(v) + f_R^{\infty} + A_R\cos(\omega v + \delta_R) \tag{3.3.7}$$

and analogously for f_I. The results for f_R are plotted in figures 3.3.3 and 3.3.5. The features of the curves are so similar to the amplitude of f_0 that we abstain from a discussion. Let us just note that again we can see a plateau for small ω where the values of the limit $\omega \to 0$ (note the colored dots) are reached, and that all curves lie on the master curve for $\epsilon = 0$ for values of ω much larger than the plateau.

The results for f_I are plotted in figures 3.3.4 and 3.3.6. The plateau value is zero for the imaginary part f_I^{∞} and A_I.

3.3.3. Limit $\omega \to 0$

For $\omega \to 0$, the analytical limits yield

$$f_0^{\omega} \to -\frac{1}{2}f_0^{\infty},\ f_1^{\infty} \to \frac{1}{2}f_0^{\infty},\ f_1^{\omega} \to -\frac{1}{4}f_0^{\infty},\ f_1^{-\omega} \to -\frac{1}{4}f_0^{\infty} \tag{3.3.8}$$

It is easy to see in the plots (figures 3.3.2 to 3.3.6) that for $\epsilon > 0$ the according values, marked by the colored dots, are approached at the plateau values, at larger ω for larger ϵ. For $\epsilon \to 0$, the long-time limit f_0^{∞} diverges with $\epsilon^{-1/2}$ and with it the others for $\omega \to 0$. It also seems clear from the plots that the onset of the plateau follows a scaling law. As mentioned before, the formulas for the limits all use $\chi(\omega)$ as input (or $\chi(2\omega)$ in case of the oscillation of f_1). So the onset of the plateau coincides the region of $\chi \propto \omega$.

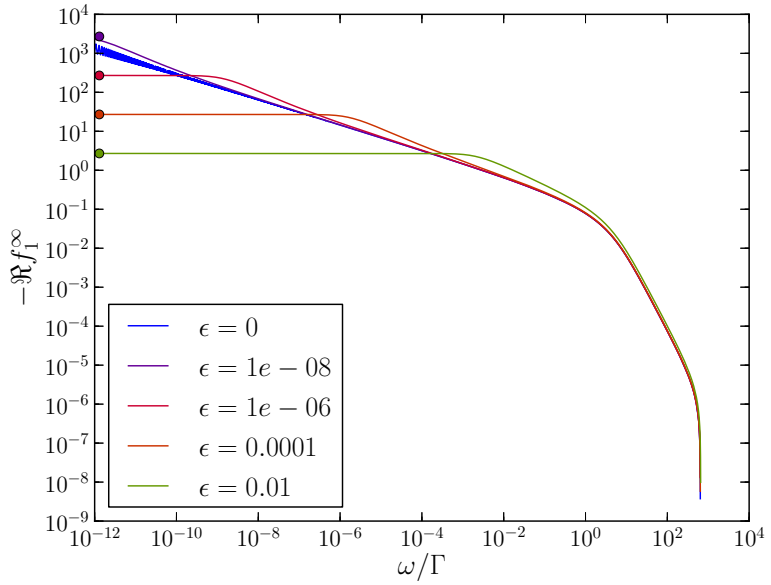

Figure 3.3.3.: The constant part f_R^∞ of the long-time limit of $f_R = \Re f_1$. The dots mark the values at the limit $\omega \to 0$ for the selected values of ϵ.

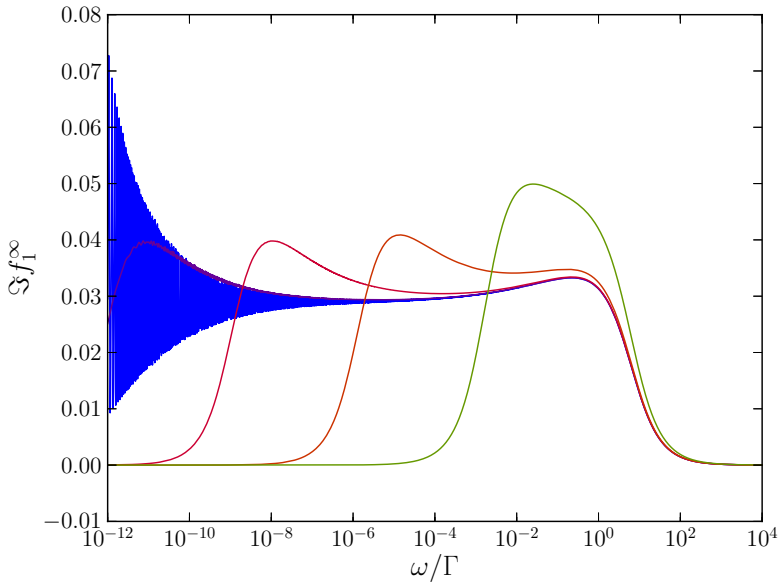

Figure 3.3.4.: The constant part f_I^∞ of the long-time limit of $f_I = \Im f_1$. The dots mark the values at the limit $\omega \to 0$ for the selected values of ϵ. See fig. 3.3.3 for the legend.

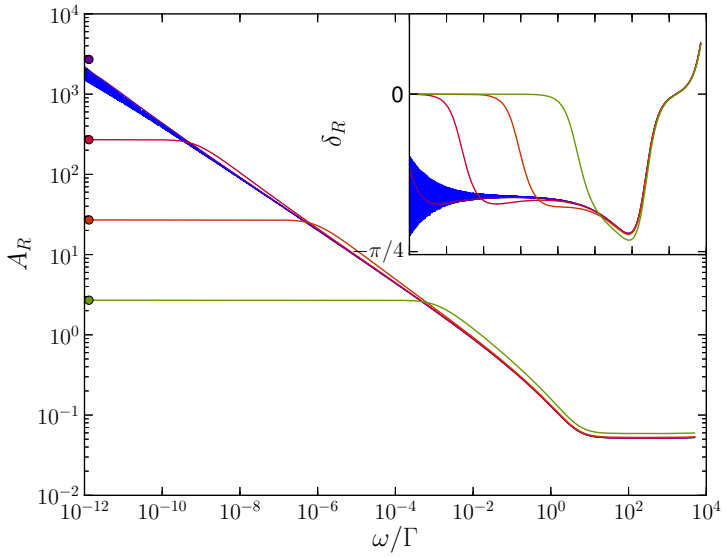

Figure 3.3.5.: Amplitude A_R of the long-time oscillation of f_R. The dots mark the values at the limit $\omega \to 0$ for the selected values of ϵ. The inset shows the phase shift δ_R, plotted over the same frequency range as the amplitude. See fig. 3.3.3 for the legend.

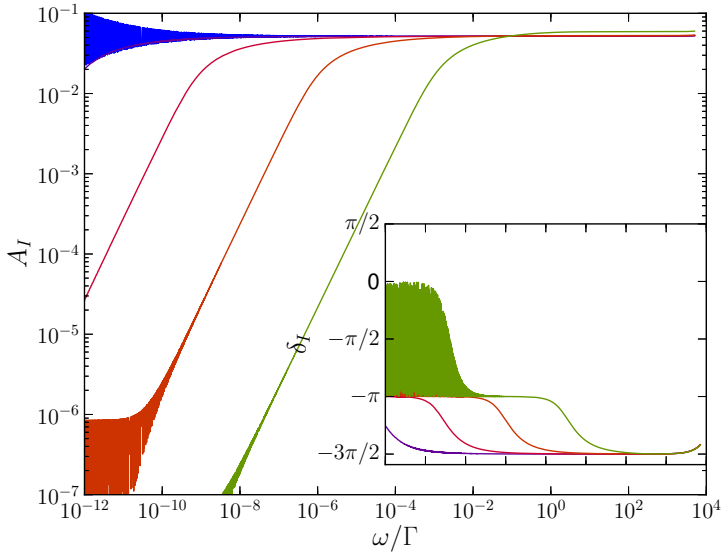

Figure 3.3.6.: Amplitude A_I of the long-time oscillation of f_I. The dots mark the values at the limit $\omega \to 0$ for the selected values of ϵ. The inset shows the phase shift δ_I, plotted over the same frequency range as the amplitude. See fig. 3.3.3 for the legend.

3.3.4. Integral version

It is possible to integrate the equation for $f_0(v)$, eq. (3.2.2), to get an integral equation, which we can analyze to verify the long-time behavior we found. Using (A.1.2), we get

$$\begin{aligned}
&f_0(v) + \int_0^v ds f_0(s)\left[1 - v_1 - 2v_2\Phi_{eq}(s)\right] \\
&\quad + \int_0^v ds f_0(s)\left[2v_1\Phi_{eq}(v-s) + v_2\Phi_{eq}^2(v-s) + 2v_2\Phi_{eq}(s)\Phi_{eq}(v-s)\right] \\
&= \int_0^v ds A(v,s) \\
&= \int_0^v ds(\cos\omega s - 2)(\dot{\Phi}_{eq}(s) + \Phi_{eq}(s)) + \cos\omega s\, m_{eq}(s) \\
&\quad - \int_0^v ds\cos\omega s m_{eq}(s)\Phi_{eq}(v-s)
\end{aligned}$$

However, as the term $-2\Phi_{eq}(v)$ in $A(v,s)$ is constant (and nonzero in a glass, $\epsilon \geq 0$) for long times, the integral diverges for $\epsilon \geq 0$. (Assuming $\Phi_{eq}(v)$ is constant for long times, it is easy to show that the other parts of the integral converge, and so cannot cancel out that term.) Nevertheless, we can use this form to confirm our long-time limit for f_0 without using a Laplace transformation. The derivation uses that the equilibrium function can be written as $\Phi_{eq}(t) = g(t) + f_{eq}^\infty$ and $m_{eq}(t) = g_m(t) + m_{eq}^\infty$, with $g(t), g_m(t) \to 0$ for long times. Simplification for long times and taking the derivative lead to

$$\begin{aligned}
&f_0'(v) + (1 - v_1 - 2v_2 f_{eq}^\infty + 2m_{eq}^\infty + 2v_2(f_{eq}^\infty)^2) f_0(v) \\
&\qquad + \int_0^\infty 2f_0'(v-s)\left(g_m(s) + v_2 g(s)\right) ds = A + \omega B_1\cos\omega v - \omega B_2\sin\omega v
\end{aligned}$$

with

$$\begin{aligned}
A &= -2\Phi_{eq}^\infty \\
B_1 &= \frac{1}{\omega}(m_{eq}^\infty + \Phi_{eq}^\infty) - m_{eq}^\infty \int_0^\infty ds\Phi_{eq}(s)\sin\omega s \\
B_2 &= -m_{eq}^\infty \int_0^\infty ds\Phi_{eq}(s)\cos\omega s.
\end{aligned}$$

This does not help much, because we are still stuck with the integral on the left-hand side we can not evaluate. But at least we can rule out a constant long-time behavior.

However, with an oscillatory ansatz

$$f_0(v) = A' + B_1'\cos\omega v - B_2'\sin\omega v$$

we can replicate the formulas we got by the Laplace transform, thus verifying the results.

3.4. Conclusion of the analytical part

In this section we have reproduced for oscillatory shear some of the results Tarzia et al. [28] showed for dielectric susceptibility. We showed in section 3.1 and 3.2 that the 2-time correlators can be split into three Fourier modes. These modes have an oscillatory long-time behavior around a constant offset for $\epsilon > 0$. For $\epsilon = 0$ the offset diverges to $-\infty$ for long times. For $\epsilon < 0$ the long-time limit is zero. (Section 3.3)

So, interestingly, we found both of the possible behaviors predicted at the start of this chapter, a finite long-time behavior for $\epsilon \neq 0$, and a diverging solution for $\epsilon = 0$.

However, as we had to assume convergent behavior for the calculation of the long-time limit, this leads to the question, whether we can trust the obtained results.

The following things are possible:

1. The Taylor ansatz might work, but the Laplace transform might have given wrong results for the long-time limit. We have confirmed the results of the Laplace transform using an integrated equation, but as we need to assume an oscillatory ansatz for this, it still wants farther proof. The most reasonable assumption for the long-time limits to be wrong, would be that the solutions diverge for long times for all $\epsilon \geq 0$, not only for $\epsilon = 0$. We will rule out this case in chapter 4 by solving the Taylor equations numerically. We can also use the numerical solution to check for errors in the calculation of the long-time values.
2. The Taylor ansatz might not work at all because the radius of convergence of the Taylor expansion for γ is zero. We will exclude this possibility in chapter 4 by looking at numerical solutions of the full model for $\gamma \to 0$.
3. The Taylor approximation might work, but only for small times. This has been found to be the case for constant shear, because there only terms γt appear: For a Taylor expansion for γ, t needs to stay small with respect to γ, so for large times the higher terms diverge, destroying the expansion. If this is the case for oscillatory shear as well, even though for all times the shear strain stays small, and we look at the full model, we might see that for some time the Taylor solution fits, and then, while the Taylor solution stays constant, the full solution decays.
   If this is the case, there might be a timescale τ that describes how long the first order Taylor expansion is valid, possibly leading to an equation of the form
   $$\Phi(t, t') = e^{-(t-t')/\tau} \left[\Phi_{eq}(t - t') + \gamma^2 \Phi_\omega(t, t')\right].$$
   We can use the Taylor approximation at $\epsilon = 0$ to start looking for such a timescale τ.

In the next chapter we will test the different possibilities mentioned here by comparing the analytical results with numerical solutions of the Taylor equations and the full model.

4. Numerical results

We will use numerical solutions of the Taylor approximation derived in the last chapter and of the full schematic model to verify our analytical expressions for the long-time behavior of the second order Taylor coefficients. This chapter consists of three parts.

In the first part, we will look at numerical solutions of the Taylor expansion, of f_0 and $f_1 = f_R + if_I$, and confirm that the long-time values of the numerical solutions converge for decreasing step size to the analytical values. We also take a look at solutions for $\epsilon < 0$ and at the relaxation of the function f_0 towards its long-time limit.

After that, we will look at solutions of the "full" schematic model for small γ to see whether the solutions show the behavior predicted by the Taylor expansion. For this, we will use a program by Joe Brader that was also used to generate results for large amplitude oscillatory shear (LAOS) [4]. We will find that the Taylor expansion is a good approximation for intermediate times, but that – at least for $\epsilon > 0$ – it is missing a decay timescale τ on which the full solution decays to zero.

In the third part, we will analyze the decay timescale of the Taylor approximation for $\epsilon = 0$ and consider possible timescales for the decay of the full solution.

4.1. Taylor solution

The main part of this section will be a comparison of the numerical solutions for $f_0(t)$ and $f_1(t) = f_R(t) + if_I(t)$ with the with the analytically predicted long-time limits. For the definition of f_0 see eq. (3.2.2), for f_1 see eq. (3.2.3). The real and the imaginary part of f_1 will be considered separately.

The code for the calculation of the Taylor coefficients, see also appendix B.2, implements a decimation method used generally for schematic MCT equations. The integro-differential equations are discretized for constant time-steps and solved iteratively for increasing time, whereby each time-step is calculated using the values calculated for smaller times because of the integrals. As this makes calculation slow for many time-steps, a decimation scheme is used, doubling the step-size every constant number of steps. Because of the oscillation we have introduced a maximal step-size, given as number of points per oscillation period N_{minp}, above which the step-size is kept constant. Obviously, this leads to slower calculations, as beyond this point the number of old points that needs to be considered for the integral

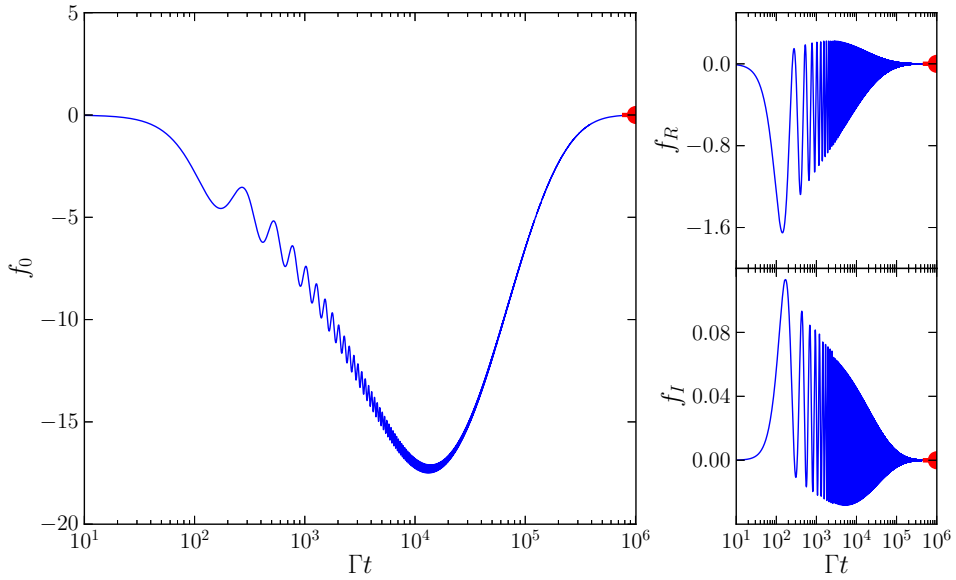

Figure 4.1.1.: Expected solution of $f_0(v)$ (big picture) for $\epsilon < 0$ ($\omega = 0.025$, $\epsilon = -0.01$). The enveloping function reaches a minimum, then goes up again to zero, with vanishing oscillation. The real part f_R and the imaginary part f_I in the small figure show some intermediary oscillation before decaying to zero. The analytical long-time limits are zero here and given as red dots.

continuously increases. We will analyze in this chapter the difference in the solutions when varying the maximal step-size. The parameters used are the distance from the glass transition ϵ, the frequency ω, the minimal number of points used per oscillation period N_{minp} and the calculated time interval.

We will concentrate on f_0 for the discussion. This has several reasons. For one, the numerical calculation of f_1 is more unstable than the one of f_0, leading to jumps especially in the imaginary part f_I of the function for small frequencies ω, probably due to the fact that all integrals contain oscillatory functions. The other reason is that the behavior of f_1 is relatively simple, as the function approaches it long-time limit smoothly and quick, while f_0 shows a richer behavior.

We will look at the three regions formed by the analytic long-time behavior separately, first we will look at the liquid region, where the functions f_0 and f_1 should converge to zero for long times, then at the glass transition point, where we expect f_0 to diverge, and then we will check the convergence of the numerics to the analytical limit for $\epsilon > 0$, where we found oscillatory solutions for f_0 and f_1.

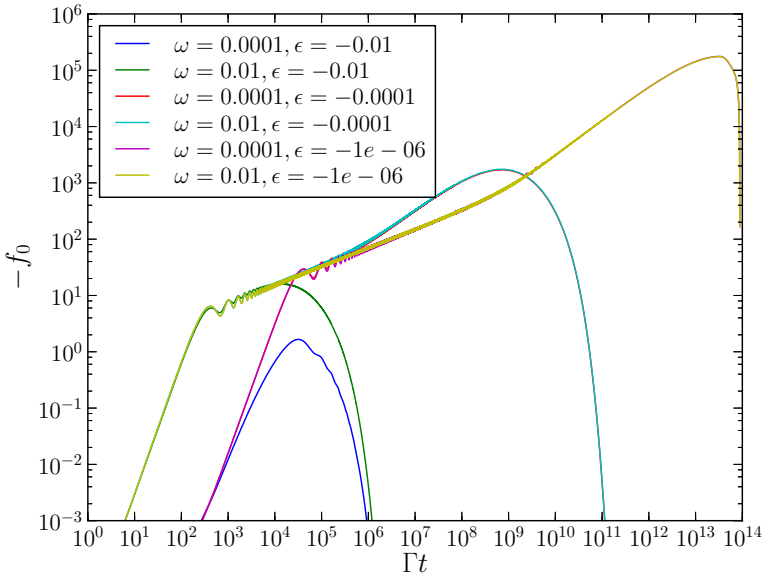

Figure 4.1.2.: Numerical solutions of $f_0(v)$ for $\epsilon < 0$ for several values of ϵ and ω. For small times, the curves with the same ω lie on top of each other, for large times the ones with the same ϵ.

4.1.1. Numerical solution of f_0 and f_1 for $\epsilon < 0$

For a liquid, $\epsilon < 0$, we expect the long-time value of f_0 and f_1 to be zero. An exemplary plot in fig. 4.1.1 shows that for long times f_0 and f_1 indeed go to zero. For intermediate times f_0 oscillates around a slower function that goes down to a minimal value until converging to zero.

Let us take a closer look at this slower function. In figure 4.1.2 several solutions for different ω and ϵ are shown in a double logarithmic plot. The curves show for large regions the same behavior. For small times, about a quarter of an oscillation period, curves with the same ω lie on top of each other. For large times all functions fall onto each other following a power law $f_0(t) \propto -t^a$, $a \approx \frac{1}{3}$ over a stretch of time before the curves with the same ϵ reach the same minimum value at the same time and then have the same timescale of relaxation toward zero. For $\epsilon \to 0$, both the absolute value of the minimum and its time increase. This lets us expect that for $\epsilon = 0$ f_0 decreases with the power law $f_0(t) \propto -t^a$, $a \approx \frac{1}{3}$ towards minus infinity. This is in accord with the analytical limit.

The offset of the numerical solutions for $f_1(t)$ is very small compared to f_0, however, the oscillation can have a finite amplitude for a considerable stretch of time.

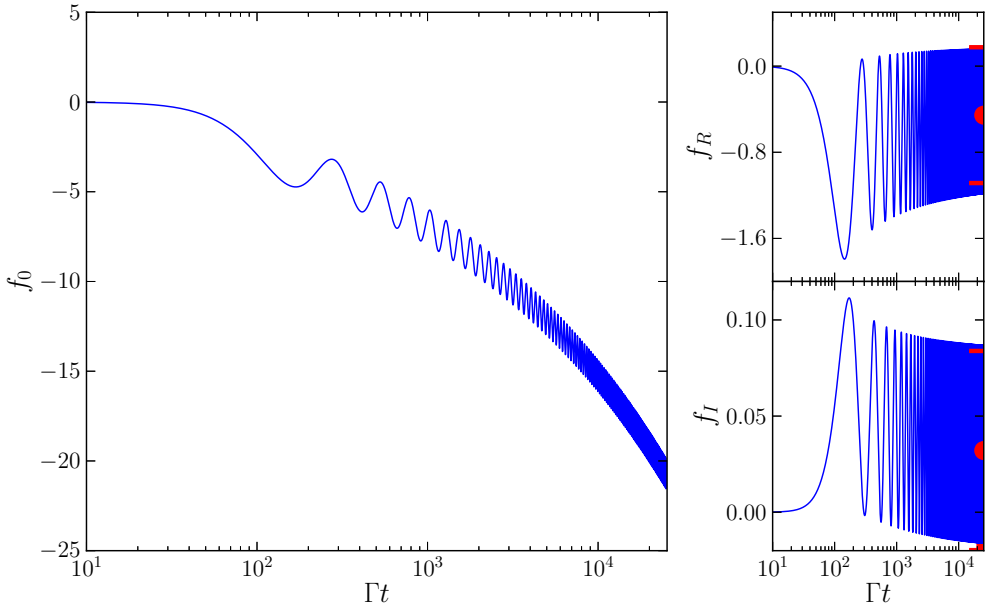

Figure 4.1.3.: f_0 and f_1 for $\epsilon = 0$ and $\omega = 0.025$. The analytical long-time limit is given as red dot at the offset with error-bars indicating the amplitude of the oscillation.

4.1.2. Numerical solution of f_0 and f_1 for $\epsilon = 0$

For $\epsilon = 0$, the analytical long-time limit for f_1 is, as for $\epsilon > 0$, an oscillation around a constant offset. For f_0, the oscillation amplitude is finite, but the whole solution goes to $-\infty$. We will come back to this case in section 4.3, when we analyze the decay timescale.

4.1.3. Numerical solution of f_0 and f_1 for $\epsilon > 0$

In fig. 4.1.4 an exemplary plot of the numerical solution of f_0 is given. The solution fits well to the analytical values for long times, given as red dot at the offset with error-bars indicating the amplitude of the oscillation. For short times, the numerical solution starts at its initial value zero and then relaxes in a couple of oscillations to the long-time value.

The shape of the solution is similar for different parameters. For parameters for which we are on the plateau in the long-time limits, the amplitude is as big as the offset, else it is smaller. The relaxation time seems to depend both on ϵ and on ω.

Rest function g_0 It is interesting to see the short time behavior of f_0, as we have no analytical information about it. In figure 4.1.5 a plot of $g_0(t)$, defined in eq. (3.3.1) as the function f_0 without the long-time oscillation, is given. As the

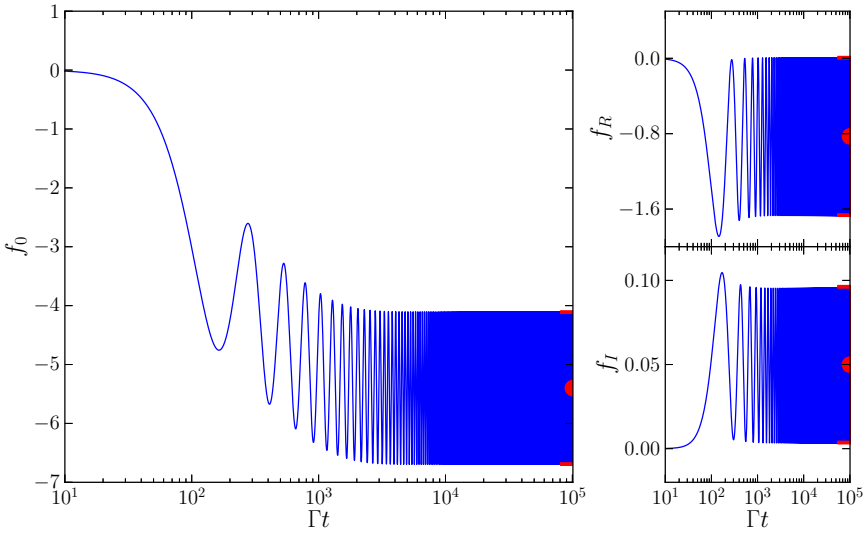

Figure 4.1.4.: A numerical calculation of f_0 and $f_1 = f_R + if_I$ with $N_{minp} = 5000$: For long times, the solution fits the analytical long-time solution. The analytical long-time limit is given as red dot at the offset with errorbars indicating the amplitude of the oscillation. ($\omega = 0.025$, $\epsilon = 0.01$)

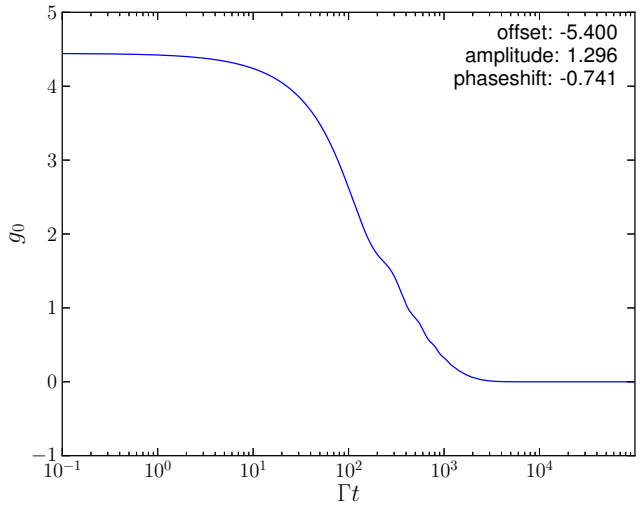

Figure 4.1.5.: Numerical result for $g_0(t)$. As the numerical amplitude deviates a bit from the analytical, a fit of the long-time values to $A+B\cos(\omega t+C)$ is used instead of the analytical long-time values, so that no oscillation remains for long times. ($\omega = 0.025$, $\epsilon = 0.01$)

numerical amplitude deviates a bit from the analytical, a fit of the long-time values to $A + B\cos(\omega t + C)$ is used instead of the analytical long-time values so that no oscillation remains for long times. The resulting parameters are given in the plot. The function relaxes smoothly from its starting value to zero.

To verify the analytical limit, we need to find out whether the plotting parameters we used for calculating g_0 actually converge to the analytical limits. So let us now take a quick look at the convergence of the numerics for small and large step-sizes. The maximal step size used in the numerical calculations is given in terms of N_{minp}, the number of points per oscillation period. Here we will look at how different step sizes influence the solution.

Large step-sizes Setting $h \to \infty$, $N_{minp} \to 0$ with $\Phi_{eq}(0) = 1$ and $\Phi_{eq}(h \cdot i) = \Phi_{eq}^{\infty}$ for $i > 0$ in the formulas describing the numerics (see appendix B.2) gives us for $\Phi_{eq}(t)$ the expected formula for long times $m_{eq}^{\infty} = \frac{\Phi_{eq}^{\infty}}{1-\Phi_{eq}^{\infty}}$, while for $f_0(t)$ we get

$$f_0(t) \to f_0^{\infty}(1 - \cos(\omega t)) \tag{4.1.1}$$

This is the analytical long-time limit of f_0 for $\omega \to 0$. So for $\omega > 0$, the step-size needs to be kept small to get the true amplitude and phase shift.

We will here look at the step-size effects for parameters $\omega = 0.025$ and $\epsilon = 0.01$ and analyze f_0. The same can be found for parameters $\omega = 10^{-6}$, $\epsilon = 0.0001$, and for f_1 in C with similar results.

Step-size effects For $\omega = 0.025$ and $\epsilon = 0.01$, let us compare different maximal step-sizes (given as N_{minp}, points per period). In fig. 4.1.4 a picture of a good numerical solution with the same parameters can be found. Fig. 4.1.6 shows the solution with the same parameters, but calculated with smaller N_{minp}. There are steps in the oscillation amplitude visible at the times where the step-size is doubled.

In fig. 4.1.7 the relative difference of the numerical from the analytical limit is calculated for a range of values of N_{minp}. For the amplitude and phase shift, the analytical limits are approached for $N_{minp} \to \infty$, as the difference goes to zero. For the offset f_0^{∞}, the difference should be zero. The difference of 10^{-6} could arise from the numerical precision of the parameters, or from numerical errors in the calculation of the analytical limit. For large step-sizes we can also confirm the prediction of eq. (4.1.1) that the values approach the analytical values for $\omega = 0$, as the red dot (analytical limit) and the green dot (numerical calculation with infinitely increasing step-size) coincide.

So on the whole we have verified the analytical limit of f_0 with the numerical calculations for the parameter values $\omega = 0.025$ and $\epsilon = 0.01$. In appendix C, the same analysis is done for f_1 at the same parameters, and for f_0 and f_1 with the parameters $\omega = 10^{-6}$ and $\epsilon = 0.0001$. For smaller ω the solutions are less stable, so they need higher N_{minp} to converge to the analytical values. Especially

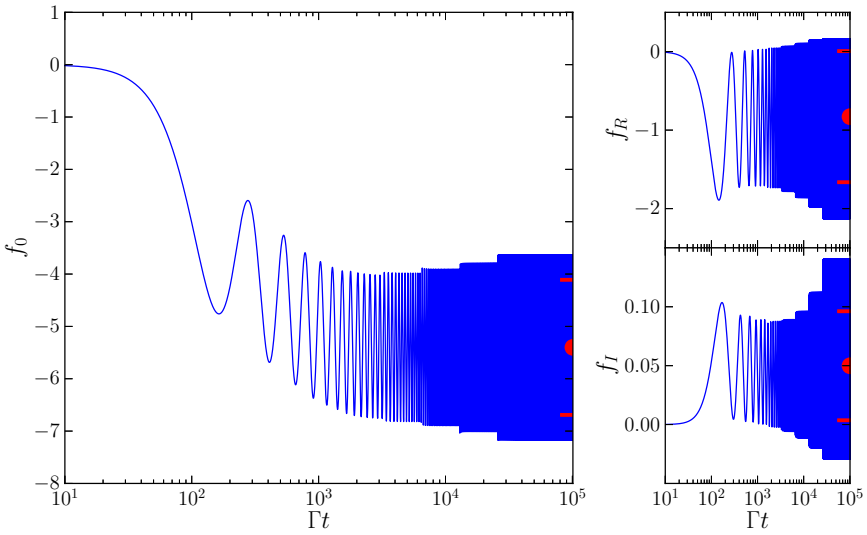

Figure 4.1.6.: A numerical calculation of f_0 and $f_1 = f_R + if_I$ with $N_{minp} = 10$: The amplitude increases with the step size. The analytical long-time limit is given as red dot at the offset with error-bars indicating the amplitude of the oscillation. ($\omega = 0.025$, $\epsilon = 0.01$)

the imaginary part of f_1 is – even for large values of N_{minp} – unstable, making an noncontinuous jump at the start of the oscillation, again see appendix C. The reason for this might be resonance phenomena, as all the terms in the integrals oscillate. However, for $N_{minp} \to \infty$ the jump gets smaller and the values converge to the analytical limit.

So we have shown that the analytical limits are true limits of the Taylor equations. With this result we rule out the first possibility mentioned in the analytical conclusion, that the analytical limits are wrong because the solutions diverge.

We have also seen that the analytical limits are actually reached relatively fast (except for $\epsilon = 0$) and, considering the numerical convergence problems, might even be a better approximation of the solution for intermediate times. We will look at this in the next section in comparison with the full schematic model.

Let us conclude this section with a numerically calculated result for the perturbation Φ_ω of the equilibrium correlator for $t' = 0$ in fig. 4.1.8. See eq. (3.2.1) for the definition. Φ_ω looks like f_0, but with additional 2ω-oscillations produced by f_1. The oscillations are stable, as a comparison of the first few oscillations with the oscillation for long times in the inset shows.

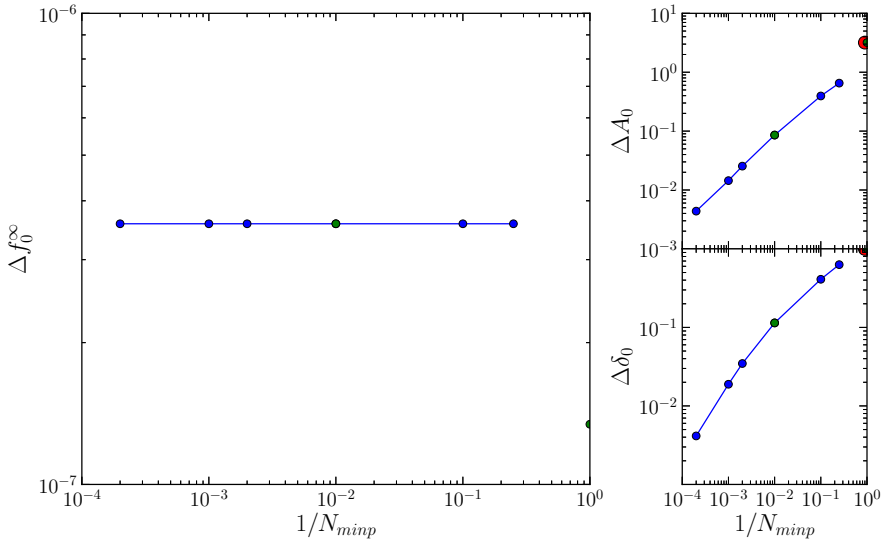

Figure 4.1.7.: Analysis of the step-size error in numerical calculations of f_0: Error of numeric value relative to analytic value of offset Δf_0, amplitude ΔA_0 and phase shift $\Delta\delta_0$ of the oscillation for long times (10^5) as function of $1/N_{minp}$. Green dot at $1/N_{minp} = 1$: infinitely increasing step size (measured at $t = 10^8$), red dots: analytically expected values for $h_{max} \to \infty$ ($\omega \to 0$), green dot at $1/N_{minp} = 10^{-2}$: measured for longer time $t = 10^6$. The constant difference in Δf_0 is probably due to numerical errors in the evaluation of the analytical limit. ($\omega = 0.025$, $\epsilon = 0.01$)

4.2. Comparison to full solution

Now we have verified the analytical long-time limit using numerical calculations of the Taylor equations, let us look at the full schematic model to see whether the solutions actually show a quadratic convergence. The solutions of the full model are calculated using numerics by Joe Brader. See [4] for more information.

In figure 4.2.1 some of the solutions we will analyze are plotted. The parameters are chosen as $\omega = 2 \cdot 10^{-5}$ and $\epsilon = 0.001$, almost on the small-frequency plateau of the analytical long-time limits of f_0 and f_1. The curves for small γ are so close to the equilibrium solution that they cannot be seen. The inset shows one of these curves, together with the equilibrium solution. While the curves for larger γ seem to have no higher harmonics, the curve for $\gamma = 0.01$ clearly shows second order terms. This is promising, as the Taylor term Φ_ω also has second order terms, as we have just seen in fig. 4.1.8.

Next, we check whether the full model converges quadraticly against the equilibrium

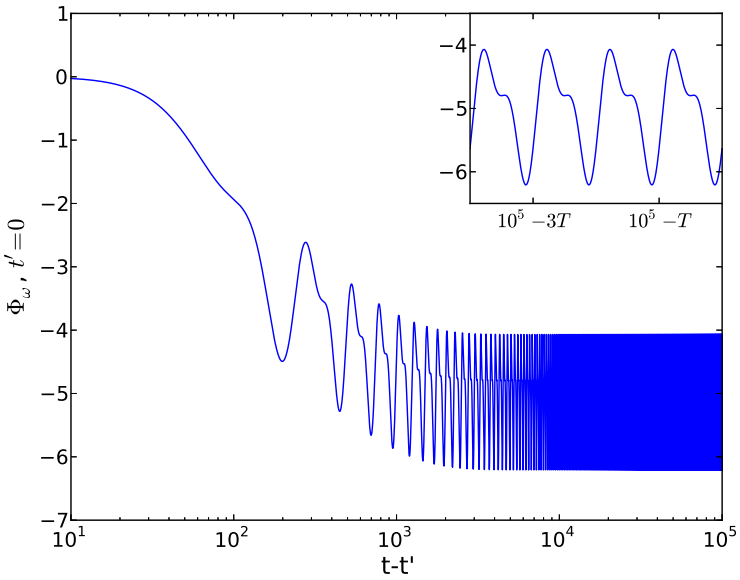

Figure 4.1.8.: Perturbation $\Phi_\omega(t,0)$ of the equilibrium correlator for small shear for $\epsilon = 0.01, \omega = 0.025$ and $t' = 0$.

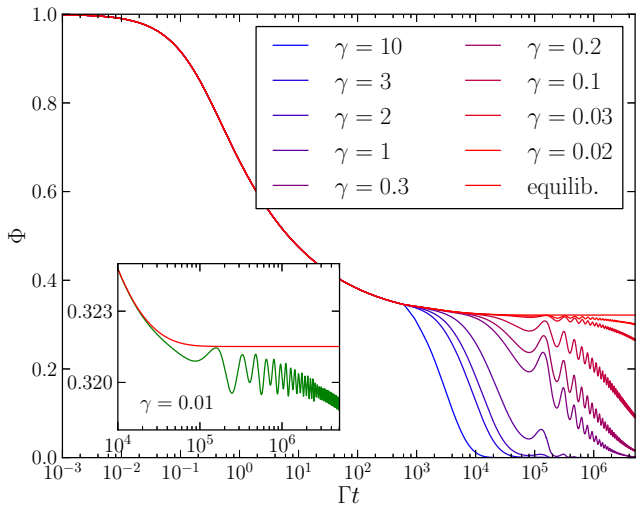

Figure 4.2.1.: Full solution for several values of γ with $\omega = 2 \cdot 10^{-5}$, $\epsilon = 0.001$ and $t' = 0$.

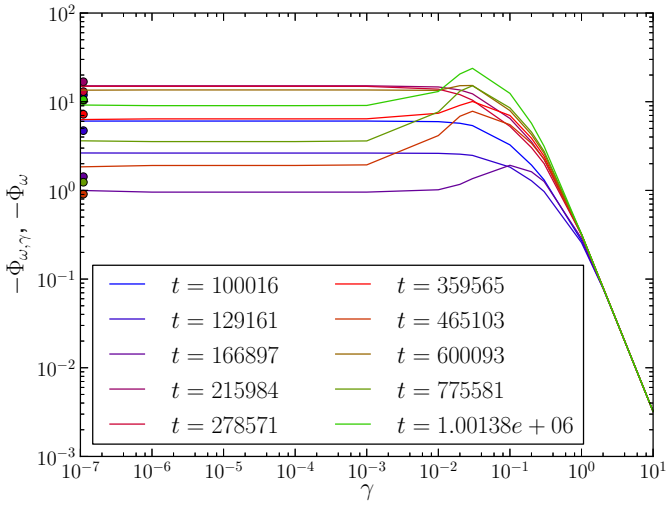

Figure 4.2.2.: Assuming $\Phi(t,t') = \Phi_{eq}(t-t') + \gamma^2\Phi_\omega(t,t') + O(\gamma^4)$, the values of $\Phi_{\omega,\gamma}(t) = (\Phi(t,0) - \Phi_{eq}(t))/\gamma^2$ (lines) should converge to $\Phi_\omega(t,0)$ (dots). The lines are for 10 fixed t-values, equidistant on a log-scale in $[10^5, 10^6]$.

solution by looking at

$$\Phi_{\omega,\gamma}(t) = \left[\Phi(t,0) - \Phi_{eq}(t)\right]/\gamma^2 \tag{4.2.1}$$

for some selected values of t and $t' = 0$, fig. 4.2.2. We take 10 values of t equidistant on a logarithmic scale in the interval $[10^5, 10^6]$. For smaller times, the difference between the curves is so small that numerical errors are a problem, especially as the equilibrium solution for $t < 2 \cdot 10^2$ is used as input. For large times, the numerics is not reliable, as, different from the Taylor solution numerics, the step-width is continuously doubled as is usually done for the equilibrium solutions. We have shown for the Taylor solutions that the amplitude of the oscillation is changed by large step-sizes, eq. (4.1.1), and it seems sensible to assume a similar behavior for the full model.

The plot clearly shows that the values are constant for small γ, a quadratic ansatz seems to hold for $\gamma < 10^{-3}$. For large γ we see a divergence $\Phi_{\omega,\gamma}(t) \propto \gamma^{-2}$ because there the solutions are already decayed to zero. For small times, there is a smooth, monotonous change from the large γ behavior to the constant limit, see for example the blue curve for $t = 100016$. For large times however, the function develops a maximum before reaching the limit, as for the orange curve with $t = 465103$. This is an interesting effect that is probably due to higher order terms.

For every time there is a dot in the same color that is the analytical limit. As the analytics only describes the long-time behavior, we might not expect the values to match the limits of the full model for small times. But even for larger times, the

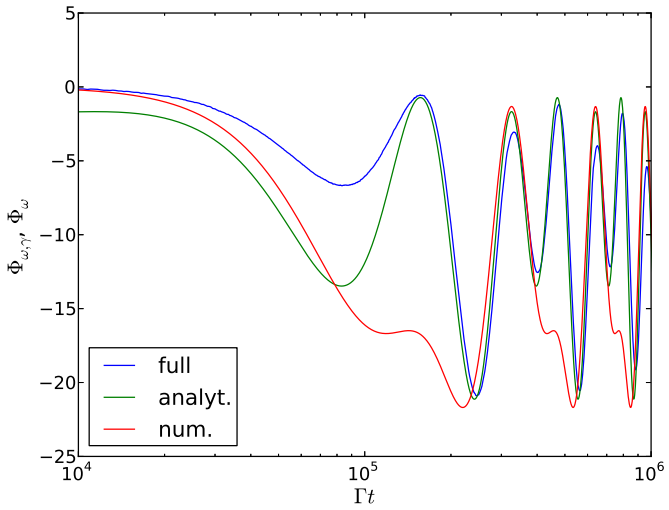

Figure 4.2.3.: Here we compare $\Phi_{\omega,\gamma}(t) = (\Phi(t,0) - \Phi_{eq}(t))/\gamma^2$ for $\gamma = 10^{-7}$ (blue) with $\Phi_\omega(t,0)$, as given by numerics (red) and the analytical long-time solution (green).

dots do not quite match the lines. But this plot is too crowded for a closer analysis, so we will look at this closer in later figures. However, the figure shows clearly that the Taylor approximation is valid and that the quadratic terms have at least the same order of magnitude as the analytical calculation. This also implies that the long-time limit already is valid for the considered time interval.

In figure 4.2.3 $\Phi_{\omega,\gamma}(t)$ is plotted for $\gamma = 10^{-7}$ in blue with the analytical long-time limit solution of $\Phi_\omega(t,0)$ in green and the numerical solution in red. The full and the analytical solution match very well. For small timescales, $t < 10^5$, some derivation is visible before the long-time limit is reached. As the frequency is so small, this only needs about half an oscillation period. After this, the solutions match well. The amplitudes of the first and second harmonics differ a bit, and some slight phase difference is visible. But the overall shape is so similar that this clearly proves our Taylor expansion works.

There are several reasons that can lead to the slight differences: First, the full curve is calculated numerically with increasing step-width, as for the equilibrium equation, ignoring the oscillation. So we expect some deviations of increasing magnitude for longer timescales. Second, we evaluated the analytical limits using numerical solutions of the equilibrium equation and performing a numerical Fourier transformation on the result. So the analytical values have some numerical errors as well.

The numerical calculations do not fit as well. The reason for this might be the instability in the calculation of f_I, the imaginary part of f_1. This seems especially probable, as the problem seems to be the second harmonic, because the main amplitude fits well, only every second oscillation is too small.

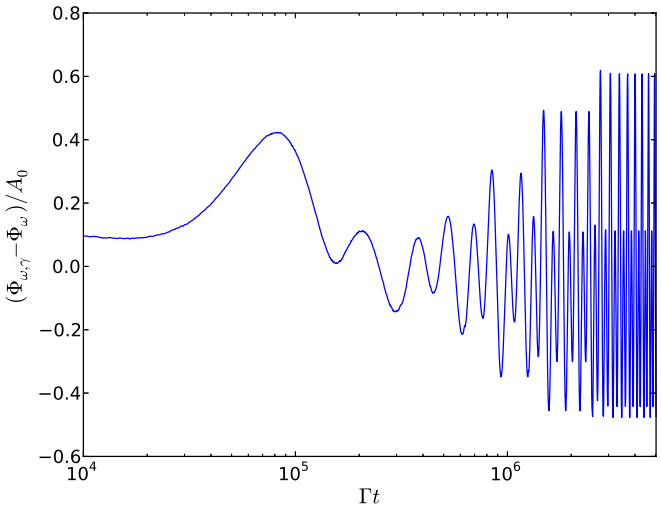

Figure 4.2.4.: Here we compare $(\Phi(t,0) - \Phi_{eq}(t))/\gamma^2$for $\gamma = 10^{-7}$ with $\Phi_\omega(t,0)$, the analytical long-time solution, by taking the difference and dividing by the analytical oscillation amplitude A_0.

In figure 4.2.4 the difference between the analytical and the full solution $\Phi_{\omega,\gamma}(t)$, $\gamma = 10^{-7}$, is plotted, normalized by the analytically expected amplitude. Fig. 4.2.2 shows that $\gamma = 10^{-7}$ is far in the quadratic regime. For $t < 10^5$, short time behavior leads to differences. For intermediate times, $10^5 < t < 10^6$, we find errors of about 20% that show as oscillations around zero. Small differences in the amplitude and phase shift of the oscillations would explain this. For large times, the differences increase, with visible steps. The reason for this is the decimation of the numerical calculation of the full solution. As we have seen for f_0 in eq. (4.1.1), this changes the amplitude of the oscillation.

In figure 4.2.5 the difference between the analytical and the full solution $\Phi_{\omega,\gamma}(t)$ is plotted again, but this time for a larger shear strain. We have chosen $\gamma = 10^{-2}$, which is right at the start of the quadratic regime, see fig. 4.2.2 , so we can take a look at the strange maxima developing at certain times before the quadratic limit is reached. For small times, $t < 2 \cdot 10^5$, the difference looks the same as for $\gamma = 10^{-7}$. However, for longer times, the full solution gets smaller than the Taylor limit. This happens even before obvious changes in the oscillation amplitude because of step-size effects set in, so we assume that it is not a numerical error, but an intrinsic phenomenon.

The explanation for this is that the Taylor solution is valid only for intermediate times, after which higher terms dominate. In fig. 4.2.4 we could not see this, because the numerical errors dominate before the non-quadratic time is reached. This result corresponds to the third possibility proposed in sec. 3.4, namely that the convergence is time-dependent, as for linear shear. We also proposed the existence

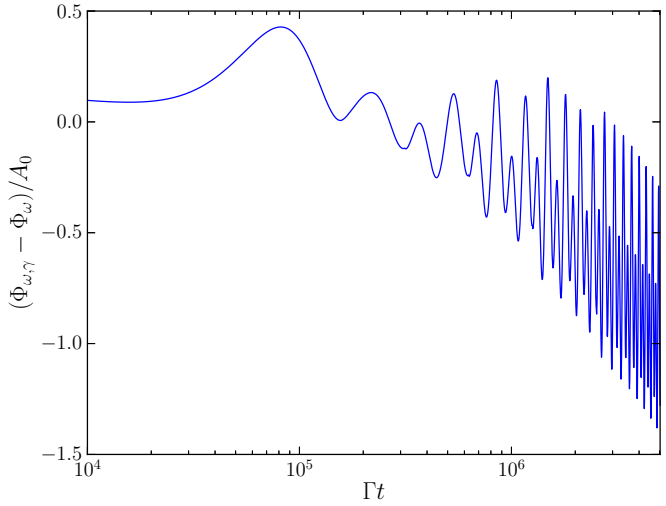

Figure 4.2.5.: Here we compare $(\Phi(t,0) - \Phi_{eq}(t))/\gamma^2$for $\gamma = 10^{-2}$ with $\Phi_\omega(t,0)$, the analytical long-time solution, by taking the difference and dividing by the analytical oscillation amplitude A_0.

of a timescale τ to describe the decay of the full solution.

4.3. Starting the search for a decay timescale

To determine the proposed decay timescale, we have three possibilities: We try to find a new analytical ansatz – a good starting point would be a beta-scaling equation, as this has been found to work for linear shear [18] –, we analyze the decay of numerical solutions of the full model and write a program that uses a maximal step-size as in the numerics of f_0 and f_1, so that numerical errors can be better controlled; or we study the decay behavior in the Taylor approximation for $\epsilon = 0$, as there the long-time limit is infinite. The underlying assumption that for $\epsilon > 0$ the decay follows the same behavior should however be tested with the full model or the beta-scaling equation.

4.3.1. Taylor approximation at $\epsilon = 0$

For $\epsilon = 0$, the analytical long-time limit for f_1 is, as for $\epsilon > 0$, an oscillation around a constant offset. For f_0, the oscillation amplitude is finite, but the solution goes to $-\infty$.

In figure 4.3.1 f_0 is plotted on a logarithmic scale for several values of ω. For short times, before the first oscillation, the curves all show the same scaling $f_0 \propto -t^a$ with $a \approx 2.28$. This is probably due to the linear regime of the oscillation. For larger

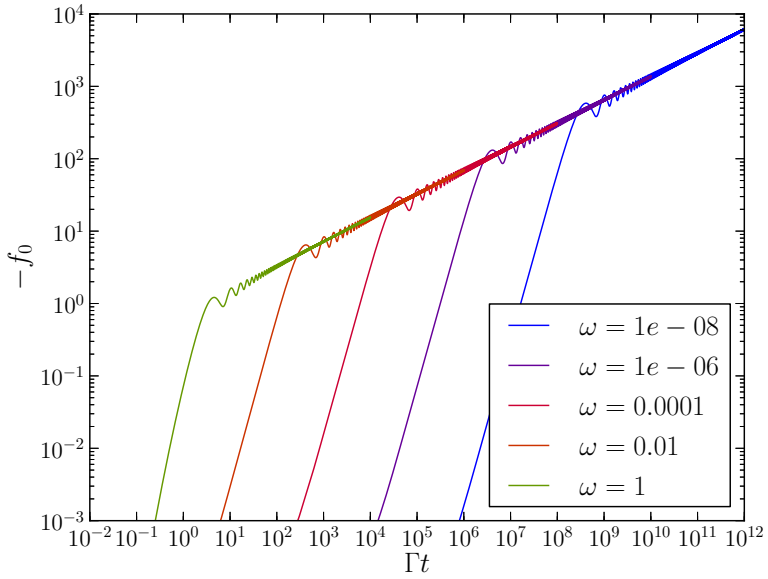

Figure 4.3.1.: Scaling in the Taylor approximation: $-f_0$ for $\epsilon = 0$. For small timescales (linear regime of first oscillation), $f_0 \propto -t^a$, $a \approx 2.28$, for long timescales $f_0 \propto -t^b$, $b \approx \frac{1}{3}$.

times, starting with about a quarter of the respective oscillation period, however, all the curves fall onto each other with $f_0 \propto -t^b$, $b \approx \frac{1}{3}$. So we get

$$\Phi(t, t') - \Phi_{eq}(t - t') \propto -\gamma^2 t^b \tag{4.3.1}$$

.

4.3.2. Full model

In fig. 4.3.2 we test the full solution for scaling analogous to the scaling found for linear shear, $\tau = 1/(\gamma\omega)$. For large amplitude shearing, the curves show scaling. This can be attributed to the fact that for large amplitudes, the shear strain behaves like linear shear for some time, during which the correlator already decays. For small shear, however, the scaling fails.

As we have found for the Taylor approximation that there the solution diverges for $\epsilon = 0$ with $\Phi(t, t') - \Phi_{eq}(t - t') \propto -\gamma^2 t^b$, we will try to rescale the full solutions with $\tau = 1/\gamma^2$. The result can be found in fig. 4.3.3. For intermediate shear amplitudes, scaling seems to work well. However, the curves for $\gamma < 0.1$ do not seem to follow the behavior very closely.

So we try another rescaling, $\tau = 1/\gamma^4$, fig. 4.3.4. While this destroys the scaling for large γ, the curves for small shear now collapse.

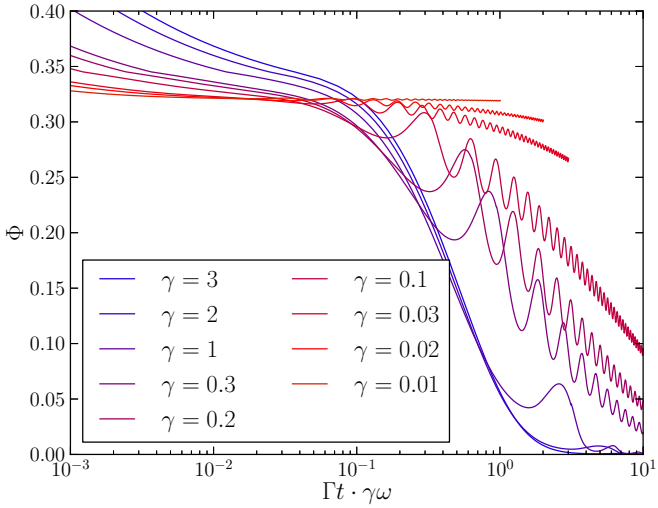

Figure 4.3.2.: The solution of the full model for $t' = 0$ and several values of γ scales like linear shear only for large shear strain. ($\omega = 2 \cdot 10^{-5}$, $\epsilon = 0.001$)

This almost seems to lead to some kind of power series description for a more complicated function. Clearly, more work is needed to figure out this interesting behavior.

In the next chapter, let us take a short look at the shear modulus for small shearing amplitude, and what we can say about its properties, especially the third harmonic, in that regime using our Taylor approximation.

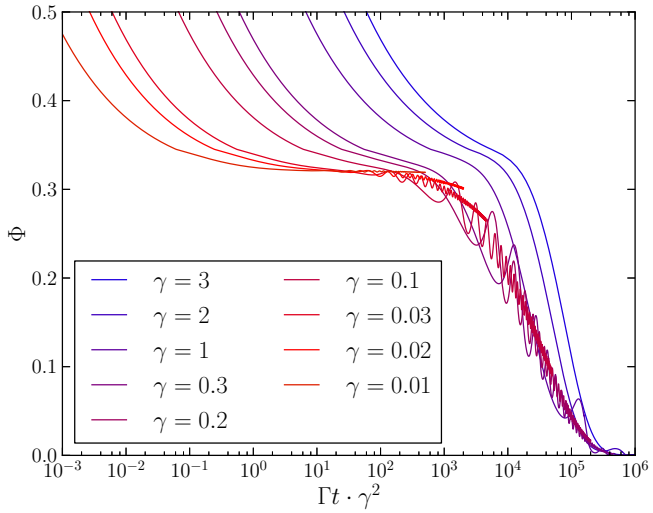

Figure 4.3.3.: The solution of the full model for $t' = 0$ and several values of γ scales with quadratic shear for intermediate shear strain amplitudes. ($\omega = 2 \cdot 10^{-5}$, $\epsilon = 0.001$)

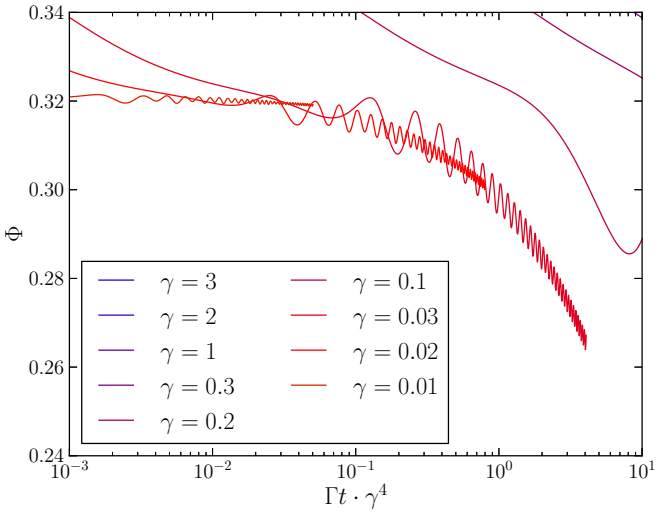

Figure 4.3.4.: The solution of the full model for $t' = 0$ and several values of γ scales with quartic shear only for small shear strain. ($\omega = 2{\cdot}10^{-5}$, $\epsilon = 0.001$)

5. Shear modulus

5.1. Theoretical results

We have found in the previous chapters that the correlator $\Phi(t, t')$ of the schematic MCT-model used by Brader can be approximated by a Taylor expansion of quadratic order. This gives us analytical results for the shear stress, including the first higher harmonic $G_3(\omega)$.

Inserting the Taylor expansion, eq. (3.2.1), into the equation for $\sigma(t)$, using eq. (2.1.3) and (2.2.10), and $v = t - t'$, gives

$$\begin{aligned}\sigma(t) &= \int_{-\infty}^{t} dt' \omega \gamma_0 \cos(\omega t') v_\sigma \Phi^2(t, t') \\ &= \frac{1}{2}\omega\gamma_0 v_\sigma \int_0^\infty dv \left(e^{i\omega t} e^{-i\omega v} + cc\right) \left[\Phi_{eq}(v) + \gamma^2 f_0(v) + \gamma^2 \left(e^{2i\omega t} e^{-i\omega v} f_1(v) + cc\right)\right]^2\end{aligned} \tag{5.1.1}$$

This, together with the analytical long-time behavior (where we skip writing every dependency on ω), lets us calculate the in eq. (2.1.5) introduced shear moduli

$$\begin{aligned}G_1(\omega) &= G_{1,eq}(\omega) + \gamma^2 G_{1,\omega}(\omega) + O(\gamma^4) \\ G_3(\omega) &= \gamma^2 G_{3,\omega}(\omega) + O(\gamma^4)\end{aligned} \tag{5.1.2}$$

Here, the term for the third harmonic is

$$G_{3,\omega}(\omega) = v_\sigma \gamma_0 i 2\omega F\{\Phi_{eq}(v) \cdot f_1(v)\}(2\omega) \tag{5.1.3}$$

$$= v_\sigma \gamma_0 \left[2 f_1^\omega \chi(\omega) + f_1^\infty \chi(2\omega) + \frac{2}{3} f_1^{-\omega} \chi(3\omega)\right]$$

$$+ v_\sigma \gamma_0 i 2\omega F\{\Phi_{eq}(v) \cdot g_1(v)\}(2\omega) \tag{5.1.4}$$

$$= G_{3,lim}(\omega) + G_{3,Rest}(\omega) \tag{5.1.5}$$

Eq. (5.1.3) is similar to an equation found for dielectric susceptibility by Tarzia et al. [28]. As found by Tarzia, we also see that this value depends on $\chi(2\omega)$, the Fourier transform of the equilibrium solution, evaluated at 2ω. We have further split the formula by inserting the long-time limit of f_1 we found in chapter 3, eq. (3.3.5). This gives us two terms, $G_{3,lim}(\omega)$ and $G_{3,Rest}(\omega)$. $G_{3,lim}(\omega)$ consists only of $\chi(\omega')$, evaluated at multiples of ω, and the long-time limit of f_1, for which we derived analytical expressions that depend again on $\chi(2\omega)$. $G_{3,Rest}(\omega)$ depends on the short time behavior g_1 of f_1, for which we have no analytical formula.

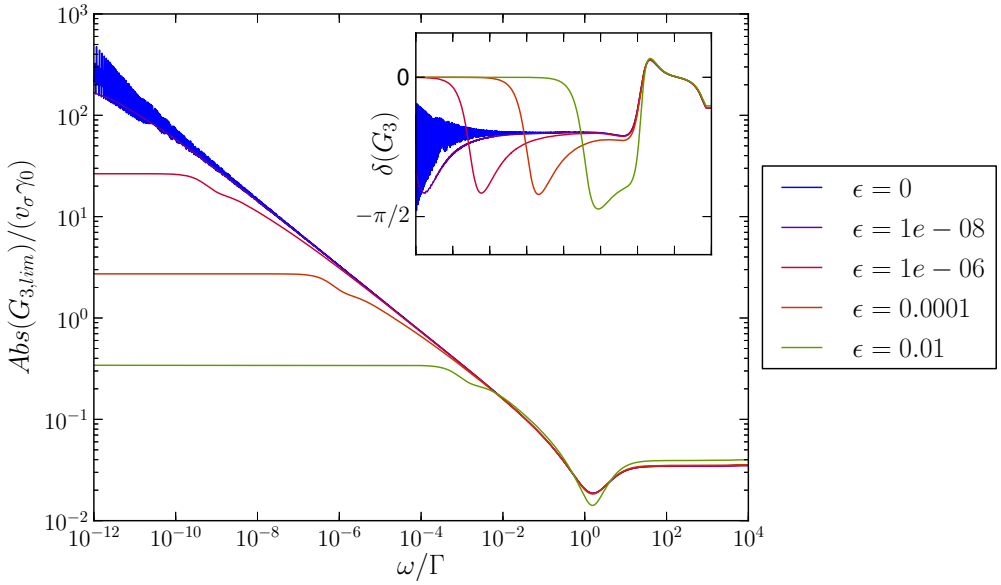

Figure 5.1.1.: Absolute value $Abs(G_{3,lim})$ and phase $\delta(G_{3,lim})$

We can calculate $G_{3,lim}(\omega)$, results are shown in fig. 5.1.1. $\chi(\omega)$ is calculated using numerics as described in appendix B.1. We can not analytically calculate $G_{3,Rest}$, as we know nothing about $g_1(v)$ except that for long times it drops to zero.

In the last chapter, we have seen that the Taylor approximation is good only for some time, until higher order terms dominate that create a decay to zero. We suggested that there is a timescale τ that describes how long the first order Taylor expansion is valid. As the timescale would probably be frequency dependent, it also would change not only the absolute value of the shear stress, but also its frequency dependency.

The first harmonic G_1 can in Taylor approximation be described by the following set of formulas:

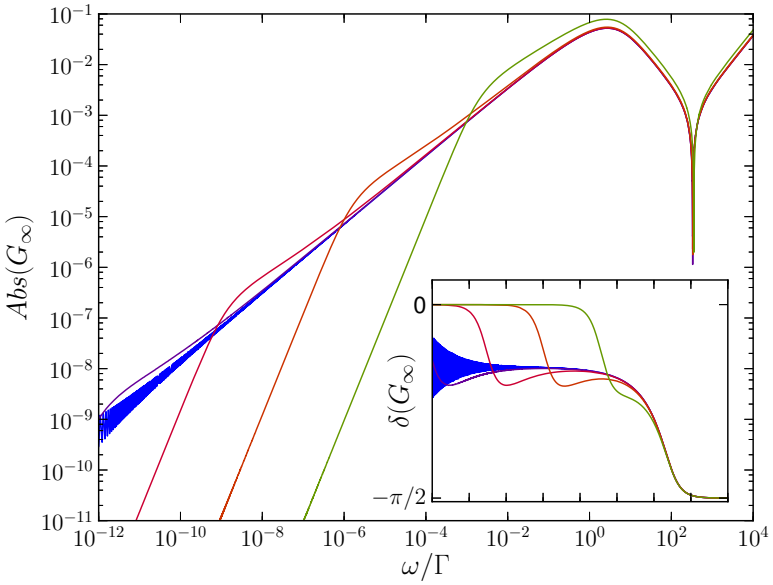

Figure 5.1.2.: Absolute value $Abs(G_\infty)$ and phase $\delta(G_\infty)$ of the prefactor in the diverging part in $G_1(\omega)$. See fig. 5.1.1 for the legend.

$$
\begin{aligned}
G_{1,eq}(\omega) &= v_\sigma \gamma_0 i\omega F\{\Phi_{eq}^2(v)\}(\omega) \\
G_{1,\omega}(\omega) &= 2v_\sigma\gamma_0 \left[f_1^\omega \overline{\chi(\omega)} + (f_0^\infty + f_1^{-\omega})\chi(\omega) + \frac{1}{2}\overline{f_0^\omega}\chi(2\omega) \right] + G_{1,Rest}(\omega) + G_{1,\infty}(\omega) \\
G_{1,Rest}(\omega) &= 2v_\sigma\gamma_0 i\omega \left[F\{\Phi_{eq}(v)\cdot g_0(v)\}(\omega) + F\{\Phi_{eq}(v)\cdot g_1(v)\}(0) \right] \\
G_{1,\infty}(\omega) &= 2v_\sigma\gamma_0 i\omega \int_0^\infty dv\, (f_0^\infty + f_1^{-\omega})\Phi_{eq}(v) \\
&= 2v_\sigma\gamma_0 G_\infty(\omega) \cdot \int_0^\infty dv\, \Phi_{eq}(v) \\
G_\infty(\omega) &= i\omega(f_0^\omega + f_1^\infty)
\end{aligned}
\tag{5.1.6}
$$

However, contrary to Tarzia, we find that the Taylor expansion for $G_1(\omega)$ is flawed, as we get a diverging term in the second order expression $G_\infty(\omega)$. In fig. 5.1.2 the result for $G_\infty(\omega)$ is shown. Only for $\omega \to 0$ the values f_0^ω and f_1^∞ cancel out, as $f_0^\omega \to -\frac{1}{2}f_0^\infty$ and $f_1^\infty \to \frac{1}{2}f_0^\infty$. As $G_\infty(\omega)$ is not zero for $\epsilon \geq 0$, we generally have $G_{1,\infty}(\omega) = \infty$, so our quadratic Taylor-term for $G_1(\omega)$ is infinite. The divergence would disappear with introducing the relaxation timescale τ. However, this would make $G_{1,\omega}(\omega)$ largely dependent on τ, so without knowing more about that timescale, it is difficult to draw any conclusion on the behavior of $G_{1,\omega}(\omega)$.

This divergence also makes the derivation of the first higher harmonic amplitude by

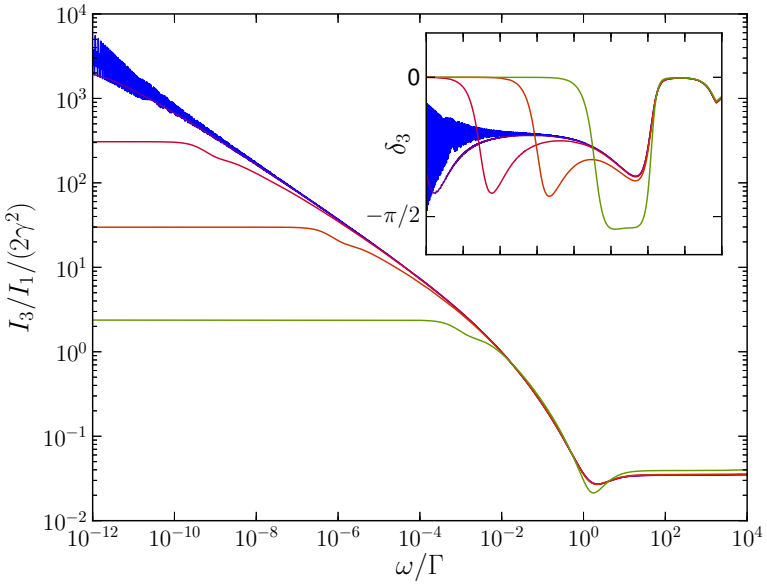

Figure 5.1.3.: Absolute value I_3/I_1 and phase δ_3. We have here ignored that $G_{1,\omega}(\omega)$ diverges, and we have assumed that $G_{3,\omega} \approx G_{3,lim}$. See fig. 5.1.1 for the legend.

Taylor expansion

$$\begin{aligned}
\frac{G_3}{G_1} &= \gamma^2 \frac{G_{3,\omega}(\omega)}{G_{1,eq}(\omega) + \gamma^2 G_{1,\omega}(\omega)} = \gamma^2 \frac{G_{3,\omega}(\omega)}{G_{1,eq}(\omega)} + O(\gamma^4) \\
\frac{I_3}{I_1} &= \left|\frac{G_3}{G_1}\right| = 2\gamma^2 \left|\frac{F\{\Phi_{eq}(v) f_1(v)\}(2\omega)}{F\{\Phi_{eq}^2(v)\}(\omega)}\right| + O(\gamma^4) \\
&= 2\gamma^2 \left|\frac{G_{3,lim}(\omega) + G_{3,Rest}(\omega)}{F\{\Phi_{eq}^2(v)\}(\omega)}\right| + O(\gamma^4) \\
&=: \gamma^2 Q_0
\end{aligned} \tag{5.1.7}$$

problematic, because we assume in the first step that $G_{1,\omega}(\omega)$ in the denominator is finite. Nevertheless, assuming the problem disappears because of τ, and that $G_{3,Rest}$ is small compared to $G_{3,lim}$, we can derived an analytic formula for the amplitude of the third harmonic shear modulus that only needs the Fourier transformation of the equilibrium correlator as input:

$$\frac{I_3}{I_1} \approx 2\gamma^2 \left|\frac{G_{3,lim}(\omega)}{F\{\Phi_{eq}^2(v)\}(\omega)}\right|. \tag{5.1.8}$$

For a plot, see fig. 5.1.3. If we use numerical calculations for f_1, we can include $G_{3,Rest}$, and the only error apart from higher order terms enters through the decay timescale.

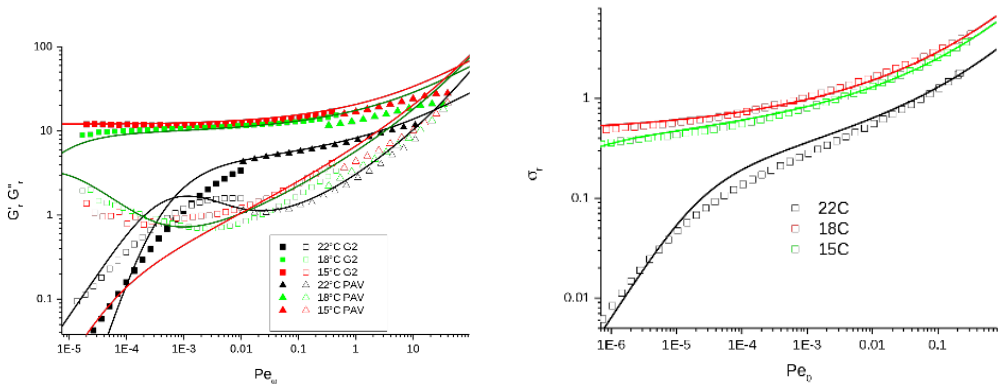

(a) Linear loss and storage shear modulus

(b) Linear shear stress

Figure 5.2.1.: Experimental results for the linear moduli with schematic MCT fits. (figure by Dimitri Merger)

5.2. Comparison to Experiment

5.2.1. Numerical results

Experiments on oscillatory shear for small amplitudes were done by Dimitri Merger in Karlsruhe at KIT. As in [4], experimental linear response values were fitted to schematic MCT parameters, yielding the following parameters:

T [deg C]	ϵ	v_σ	Γ	γ_c	η_∞
22	-0.003	55	100	0.22	0.66
18	-3.00E-04	115	105	0.20	1.04
15	5.00E-05	135	105	0.20	1.13

In fig. 5.2.1 the experimental linear moduli are shown together with the fit results. The experimental results for oscillatory shear with small amplitudes normalized by the quadratic shear amplitude are visible in fig. 5.2.2. For small amplitudes, a plateau is found, as predicted by the analytical results in this thesis.

An analysis of the plateau heights for different temperatures and frequencies gives fig. 5.2.3.

5.2.2. Analytical results

As a test, we first reproduce the fits of the linear shear moduli of fig. 5.2.1 with the same parameters, see the small plot in fig. 5.2.4. To reproduce the curves, we had to plot G_1 over ω instead of $Pe_\omega = \frac{\omega}{\Gamma}$. Now we use eq. (5.1.3) to numerically calculate a curve equivalent to 5.2.3. In the large plot of fig. 5.2.4, f_1 as input for the Fourier transform was calculated with step-size $N_{minp} = 10$ (10 points per

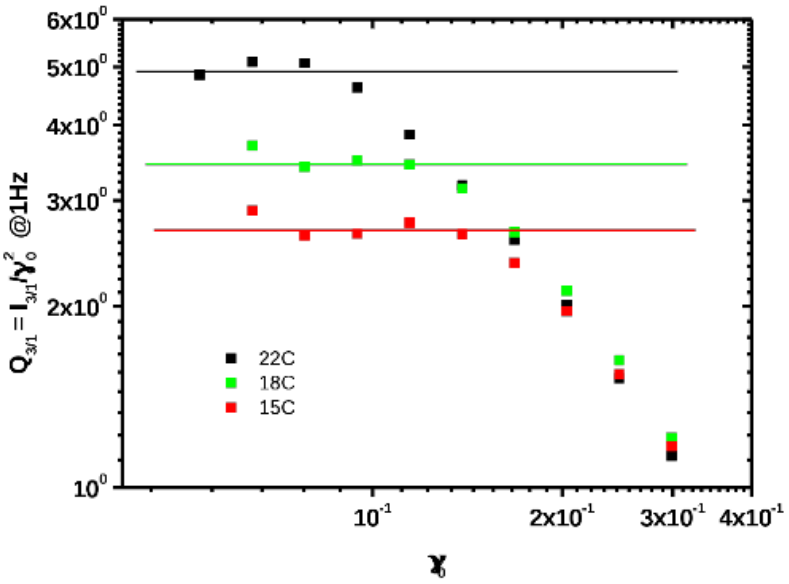

Figure 5.2.2.: Relative amplitude of the first higher harmonic stress for small shearing amplitudes. (figure by Dimitri Merger)

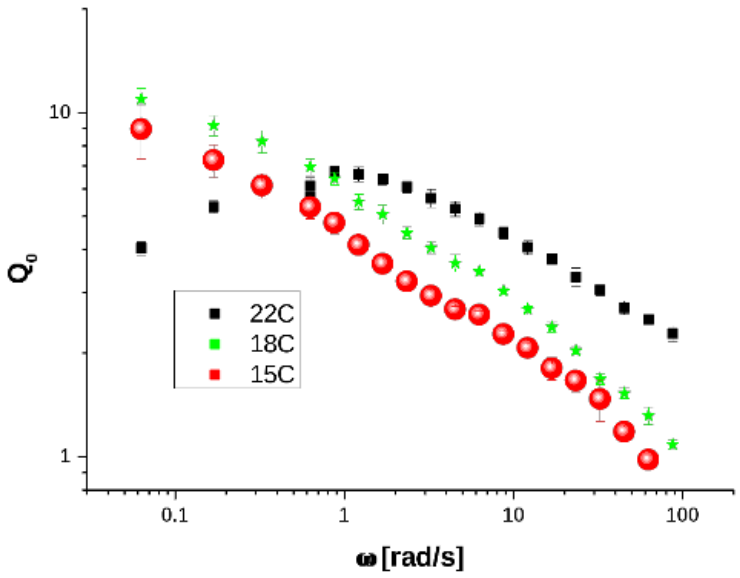

Figure 5.2.3.: Experimental results of Q_0 for small shear strain (figure by Dimitri Merger)

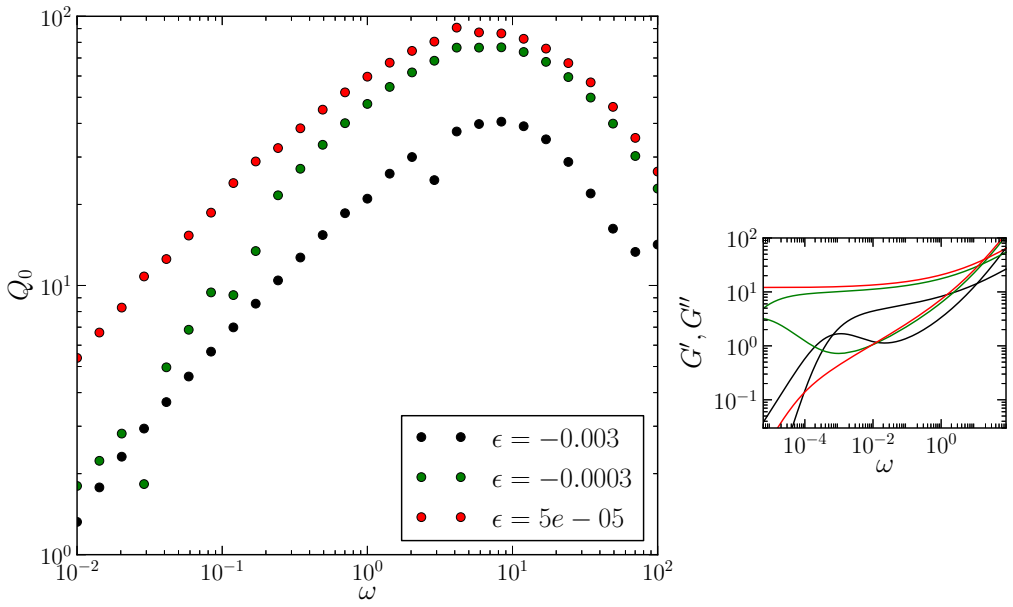

Figure 5.2.4.: Q_0, calculated with the Taylor approximation with smaller step-size but smaller time-interval ($N_{minp} = 10$, calculation time 1000 periods for each f_1). Small plot: Reproduction of the schematic MCT fits in fig. 5.2.1 with the parameters given in the table. To reproduce the curves, we had to plot G_1 over ω instead of $Pe_\omega = \frac{\omega}{\Gamma}$.

oscillation period) and we have calculated 1000 periods for every set of parameters. For $\epsilon = 5 \cdot 10^{-5}$, the glassy curve, this can lead to errors: First, because we just cut off the long-time limit, and secondly, the long-time limit oscillates, which is not considered for in the numerics for the Fourier transform. For the other two liquid values $\epsilon < 0$ we just have to hope that the long-time limit zero is reached fast enough. As we have seen, the relaxation times diverge for $\epsilon \to 0$, so we expect to get the most trustworthy results for $\epsilon = -0.003$.

The behavior of these results is very different from the ones calculated using only the long-time limits, fig. 5.1.3. There are several reasons for this: First, two of the curves presented here are for liquid parameters, $\epsilon < 0$, so the analytical long-time limit results there are zero, and the rest is ignored for calculating the values in fig. 5.1.3. We see at the one glassy curve (the red dots), that there the behavior deviates as well. For large frequencies, the qualitative behavior is the same (Q_0 decays for increasing ω), but for small frequencies the plateau created by the long-time values is destroyed, and instead Q_0 decays for $\omega \to 0$. A study of g_1 and its scaling behavior might shed some light on this.

A comparison with the experimental results show that the shape of Q_0 and its order of magnitude is similar to the experimental results, where the black dots shows also

a maximum for intermediate frequency. This dependence on ϵ, however, is very different than in the experiment: There, an increase in epsilon leads to a decrease in Q_0 for $\omega > 1$, while in fig. 5.2.4, an increase in ϵ leads to an increase in the amplitude of the third harmonic in relation to the first.

To conclude, the comparison shows some interesting features in Q_0, but is by no means complete. It might be worthwhile to repeat the numerical calculation with a smaller step-size and a better adapted Fourier transform, or by using the analytical long-time values and only numerically calculate the rest function g_1. For this, it might also be interesting to study g_1 and its dependence on ϵ and ω. However, we showed here that the Taylor approximation can be used to calculate higher harmonics of the shear stress, and thus goes beyond linear response.

6. Conclusion

In this thesis we studied the decay of correlators for large times and small oscillatory shearing amplitudes by looking at a Taylor approximation of the equilibrium correlator. We took a schematic model without time translational invariance for oscillatory shear in two time variables t and t' to get results for the higher harmonics of the shear stress.

Inserting a Taylor expansion ansatz yielded an equation for the second order Taylor approximation for small shearing amplitudes. For this equation, we needed the solutions of two linear integro-differential equations, f_0 and f_1, which correspond to the first two coefficients of a Fourier series in terms of the sum $t + t'$ of the time variables. Both solutions thereby depend on the difference $t - t'$ of the time variables only. This corresponds to results from Tarzia et al. for dielectric susceptibility[28].

We analyzed the long-time behavior of the two functions, and found oscillatory solutions for both of them. Amplitude and offset of the oscillations depend on the distance from the glass transition ϵ. In a liquid, the solutions decay to zero. In a glass, the oscillations parameters are finite. Directly at the glass transition, for $\epsilon = 0$, the offset of the function f_0 is minus infinity, leading to a diverging solution.

The long-time limits depend on the applied frequency ω. For $\epsilon > 0$ the zero-frequency limit is approached for finite frequencies, thus forming a plateau. For frequencies larger than the plateau onset, the curves for different ϵ lie on a common curve. For $\epsilon \to 0$, this curve stretches to infinity for $\omega \to 0$, while the other curves divert to their plateau value. This behavior is universal among the different limits (except the imaginary part of f_1). The behavior can be attributed to the fact that the Fourier transform $\chi(\omega)/\omega$ of the equilibrium curve also reaches a plateau value there, as the limits depend on it.

We verified the analytically calculated formulas for the Taylor approximation and their long-time limits in two ways: First, we numerically solved the equations for the Taylor coefficients f_0 and f_1. We could see the predicted behavior and checked for proper convergence of the long-time limits for different step-sizes. We also compared the limits with numerical solutions of the full schematic model, which showed that there is a time interval for which the approximation works well. For large times, however, the full solutions show a decay on time-scale τ we cannot replicate with the Taylor approximation.

To find τ, we analyzed the numerical solutions of f_0 for different ω at the glass transition, $\epsilon = 0$. We found that after $T/4$, the curves collapsed onto each other, following a power law $f_0 \propto -t^{\frac{1}{3}}$. This leads to $\Phi(t, t') - \Phi_{eq}(t - t') \propto -\gamma^2 t^{\frac{1}{3}}$ for the full solution. However, rescaling the full solution for $\epsilon = 0.001$ with γ^2 gave good

scaling results only for intermediate values of γ. For very small γ, scaling with γ^4 seemed to yield better results.

This might indicate, together with the scaling $\propto \gamma$ for large values of γ, that the scaling does not follow a simple power law, but some more complex function.

Ignoring the decay time, we inserted the Taylor approximation into equations for the shear stress. This gave an equation for the third harmonic $G_3(\omega)$. $G_3(\omega)$ depends on the Fourier transform of f_1 times the equilibrium correlator, evaluated for 2ω. We can solve this using the long-time values and $\chi(\omega)$, except for some rest function that depends on the short time behavior of f_1. Again, this relates to previous results for dielectric susceptibility[28].

We also get a perturbation term of the equilibrium result for G_1. However, ignoring the relaxation time we get a diverging term in the expression. Assuming that the divergence will be fixed by the relaxation time, and that otherwise the effects of this time-scale are negligible has given us a formula for the amplitude of the first higher harmonic versus the base frequency, I_3/I_1.

This could be compared with some experimental results by Dimitri Merger (KIT).

To conclude, we showed in this thesis that the Taylor approximation works for intermediate time-scales and we managed to study analytically some higher harmonic results of oscillatory shear. The open question remaining is that of the time-scale τ. There are several possibilities to analyze it:

First, the Taylor approximation for $\epsilon = 0$ has a diverging term that leads to a relaxation time, as we have shown. However, it should be checked with an additional method that this indeed gives the right scale for $\epsilon = 0$, as this relaxation time could be masked by a smaller decay time by the higher order terms as the rescaling results for the full model at $\epsilon = 0.001$ indicate.

Second, the decay of the full model could be analyzed, as we have started here. However, some work has been done during the time of the thesis towards a program with controllable maximal step-size, providing a starting point for further investigation.

Third, a different kind of approximation approach, a beta-scaling equation that approximates the full solution for long times and small parameters ϵ and γ, might yield some analytical answers.

So, though much has been done towards understanding small amplitude oscillatory shear, the central question "Does a glassy system liquify for small oscillatory shear, and on which time-scale?" remains open.

A. Miscellaneous maths

A.1. Convolution

Definition (one-sided):

$$(f \star g)(t) = \int_0^t ds f(s) g(t-s) \tag{A.1.1}$$

The convolution is symmetric, $(f \star g)(t) = (g \star f)(t)$.
Nice trick to pull a differentiation out:

$$\int_0^t ds f(s) g'(t-s) = \frac{d}{dt}[\int_0^t ds f(s) g(t-s)] - f(t)g(0) \tag{A.1.2}$$

Prove by calculating $\frac{d}{dt}[\int_0^t ds f(s)g(t-s)]$.

A.2. Laplace transform

The standard definition of the Laplace transform is used, not the alternative version often used in MCT. This makes it easier to use different kinds of literature.

$$F(p) = LT\{f(t)\}(p) = \int_0^\infty dt e^{-pt} f(t) \qquad , f : \mathbb{R}_{\geq 0} \to \mathbb{C} \tag{A.2.1}$$

The Laplace transform is linear and defined for positive values of t only. It has the following properties:

$$LT\{e^{-bt} f(t)\} = F(p+b) \qquad , b \in \mathbb{C} \tag{A.2.2}$$

$$LT\{f'(t)\} = pF(p) - f(+0) \tag{A.2.3}$$

$$LT\{f_1 \star f_2\} = F_1(p) \cdot F_2(p) \tag{A.2.4}$$

If a long-time limit exists, it can be calculated via the Laplace transform:

$$\lim_{t \to 0} f(t) = \lim_{t \to \infty} pF(p) \tag{A.2.5}$$

The Laplace transform is connected to the Fourier transform with $p = i\omega$. For the Laplace transform, the function $f(t)$ only needs to be defined for $t > 0$, while for the Fourier transform, we need $t \in \mathbb{R}$, we can decide how to extend $f(t)$. We will use here $f(t) = 0, t < 0$. This gives us

$$FT\{f(t)\}(\omega) = F(i\omega) \forall \omega \in \mathbb{R} \tag{A.2.6}$$

B. Numerical methods

B.1. Fourier transform

Here some information about doing the Fourier transform of $\Phi_{eq}(t)$ to $\chi(\omega)$ will be given. As Φ_{eq} varies on a logarithmic scale, and usually the time range is thus also on some kind of logarithmic scale, the established methods for Fourier transformations, like Fast Fourier Transform, do not work, as they need data on a linear time range. The naive solution, interpolation, fails, because to capture the fast decay of the correlator for small times, the step-size h needs to be really small. But to include the slow decay of the function for long times, the time interval T needs to be big. This can lead to something like $T/h \approx 10^{10}/10^{-5} = 10^{15}$ values, so that the array would take 3 Terabyte.

There are some codes out there that deal with non-equidistant Fourier transforms. However, most use the minimal step-size h and T to determine the range of ω. This leads to very small ranges of ω very close to zero.

But we know that $\Phi_{eq}(t)$ has relevant dynamics on large as well as small timescales, so we expect the same for $\chi(\omega)$. It turns out that the easiest way to get a logarithmic scale in frequency-range is to interpolate the calculated values of $\Phi_{eq}(t)$ linearly, do the Fourier transform on these linear bits, and sum the terms up. The Fourier transform of a linear function can be solved analytically, leading to an expression only of the calculated values. This has been done already in [19], eq. 4.5 et seq., so here we show some basic python code for demonstration. The code is fully functional, but to use the full potential it should be changed to accept arrays of omega-values, so that the sine and cosines can be reused.

Some details for the python-unused reader: np.diff creates just an array of the differences between the input array of the same size minus 1 (dt[i]=t[i+1]-t[i]). a negative index counts backwards from the end of the array, starting with -1, so indexes of arrays go from 0 to -1. The imaginary unit is j. Everything else, like that multiplication of arrays is point-wise, is pretty much like Matlab.

```
'''Calculate Fourier transform using linear interpolation in time
Input:
  t, phi should be arrays, phi[i]=phi(t[i]), omega a scalar.
  If phi has a nonzero long-time limit,
    phi_inf should be set with it
  For correlators of schematic MCT,
    t should be given on a roughly logarithmic scale
Returns:
```

```
    omega, Fourier transform of phi evaluated at omega
    '''
def fourier(t, phi, omega, phi_inf=0.):

    dphi = np.diff(phi)
    dt = np.diff(t)
    g = dphi/dt
    S = np.sin(f*t)
    C = np.cos(f*t)
    dS = np.diff(S)
    dC = np.diff(C)

    chi1 = phi[0]*C[0] - phi[-1]*C[-1] + 1./omega * sum(g*dS)
    chi2 = phi[-1]*S[-1] - phi[0]*S[0] + 1./omega * sum(g*dC)
    chi1 += phi_inf

    return omega, chi1 + 1j* chi2
```

B.2. Calculating correlators of schematic models

Here we describe how to calculate the schematic MCT correlators $\Phi_{eq}(t)$, see eq. (2.2.1) for the definition, $f_0(t)$ and $f_1(t)$, see eq. (3.2.2) and (3.2.3). The method for the equilibrium correlator Φ_{eq} is one of the standard methods used [30].

For the numerical calculation of $f_0(t)$ and $f_1(t)$, we will use standard discretization of time, but as Φ_{eq} changes on a logarithmic scale and our solutions $f_0(t)$ and $f_1(t)$ depend on it, we will start with a small step-width h_{min}, and then double it several (m_{stop}) times, until we reach a final step-width $\frac{\omega/2\pi}{N_{minp}}$, so that we can still resolve the oscillation of our solution with N_{minp} points. For the rest of the calculation we keep the step-width constant. The derivative of ϕ_{eq} is calculated by spline interpolation.

B.2.1. Numerical setup

Convolution All needed convolutions can be brought to the form

$$\int_0^t ds f'(s) m(t-s).$$

We can split this into intervals of size h (with $t = t_i = h \cdot i$),

$$\int_0^t ds f'(s)m(t-s) = \sum_{j=0}^{i-1} \int_{t_j}^{t_{j+1}} ds f'(s)m(t_i - s) \approx \sum_{j=0}^{i-1} m(t_{i-j}) \int_{t_j}^{t_{j+1}} ds f'(s)$$
$$\approx \sum_{j=0}^{i-1} m(t_{i-j})(f(t_{j+1}) - f(t_j)).$$

The only assumption here is that $m(t)$ is a slowly varying function with respect to h that can be approximated by the upper boundary. We take the upper boundary, because for the convolutions we want to calculate, $f(t)$ is a function of $\Phi_{eq}(t)$, so the absolute value of its derivative is monotonously going to zero. Thus for every interval, the later values of $m(t)$ will be weight stronger.

In case $m(t-s)$ also is a function of $\Phi_{eq}(t-s)$, it might have fast varying parts for $s \approx t$. For large s, $\Phi'_{eq}(s)$ is very small, so that this will not result in a big error, as long as t is big enough. So for small t we need a small step-size. For large t, the step-size just needs to be big enough that $m(t)$ can be considered slowly varying. This means that we want some kind of decimation.

Decimation We double the step-size every N_{double} points. For this, starting with $t_0 = 0$, we take every $2n$-th value so that the former calculated values have the same step-size.

As we expect f_0 and f_1 to be oscillating functions with frequency ω for long times, and we assume them to be slowly varying over h, we can only decimate to a maximal step-size, so that we still have N_{minp} points per period. For Φ_{eq}, we can decimate as many times as we want.

Discrete differentiation The derivation is discretized as $f'(t_i) \approx \Delta_i f(t_i) + \Delta$, with $\Delta_i = 3h/2$, $\Delta = \frac{f_{i-2} - 2f_{i-1}}{h}$

B.2.2. Calculating the equilibrium correlator

It is important to use a numerical discretization that leads for long times to the long-time equation for Φ_{eq}^{∞}, eq. (2.2.4), so that we get the right long-time limit [Th. Voigtmann, private communication]. We checked this for the following pseudo-code. Also, different to $f_0$and f_1, the resulting discrete equation for Φ_{eq} is quadratic (hidden in the memory function m). Solving this with a formula is numerically too unstable (for stability purposes, the numeric approximation should never be less than the analytic value, else the solution decays to zero), so the quadratic equation is solved iteratively.

```
# initialize with linear extrapolation
cpdef initialval_eq():
```

```
    for i in xrange(N):
        phi[i] = 1. - i*h
        m[i] = v1*phi[i] + v2*phi[i]**2

# decimate - take every second value
def new_stepwidth():
    phi[:dN] = phi_old[::2]
    m[:dN] = m_old[::2]

def main():
    # create arrays, input parameters
    init()
    N = N_double
    h = h_min
    dN = 0
    # iterate over decimations
    for i in xrange(m_stop + 1):
        phi, m = new_stepwidth()
        calc_eq()
        h = 2.*h
        dN = (dN + N + 1)//2

# calculate values for i in range(dN, dN + N)
def calc_eq():
    if dN == 0:
        phi, m = initialval_eq()
        return
    b = 1. - phi[0]
    a = 1. + 1./h + m[0]
    for i in xrange(dN, dN + N):
        # accounting for end points of convolution and derivation
        c = -(1./h + m[0]) * phi[i-1]
        # convolution
        for k in xrange(1, i):
            c += (phi[k] - phi[k-1]) * m[i-k]
        # iteration to solve quadratic equation
        phi0 = phi[i-1]
        m0 = v1 * phi0 + v2 * phi0**2
        phi1 = 1./a * (b*m0 - c)
        k = 0
        while abs(phi1 - phi0)/abs(phi0) > 1e-10 and k<k_max:
            k += 1
            phi0 = phi1
             m0 = v1 * phi0 + v2 * phi0**2
            phi1 = 1./a * (b*m0 - c)
        phi[i] = phi1
        m[i] = v1 * phi[i] + v2 * phi[i]**2
```

B.2.3. Calculating the Taylor solution

The equations for f_0 and f_1 are reformulated for the numerical solution by introducing new memory functions m_0 and m_1 that mix the homogeneous and the inhomogeneous parts to speed up the calculation of the convolution.

$$\begin{aligned} 0 &= f_0'(v) + (1 + v_1 + v_2)\, f_0(v) + (2 - \cos\omega v)\left[\Phi_{eq}'(v) + \Phi_{eq}(v)\right] \\ &\quad + \int_0^v ds \left[m_0(v-s)\Phi_{eq}'(s) + v_2 f_0(v-s)\left(\frac{d}{ds}\Phi_{eq}^2(s)\right)\right] \\ m_0(v) &= m_{eq}(v)\cos(\omega v) + 2 f_0(v)\left[v_1 + v_2\Phi_{eq}(v)\right]. \end{aligned} \tag{B.2.1}$$

$$\begin{aligned} 0 &= f_1'(v) + (1 + v_1 + v_2 + i\omega)\, f_1(v) \\ &\quad + \frac{1}{2}\left(1 - e^{i\omega v} - \frac{1}{2}e^{-i\omega v}\right)\cdot\left[\Phi_{eq}'(v) + \Phi_{eq}(v)\right] \\ &\quad + e^{-i\omega v}\int_0^v ds\, e^{i\omega(v-s)} f_1(v-s) m_{eq}'(s) + e^{i\omega v}\int_0^v ds\, m_1(v-s)\Phi_{eq}'(s) \\ m_1(v) &= e^{-i\omega v}\left[\left(v_1 + 2v_2\Phi_{eq}(v)\right) f_1(v) + \frac{1}{2} m_{eq}(v)\left(\frac{1}{2}e^{-i\omega v} - 1\right)\right]. \end{aligned} \tag{B.2.2}$$

Here pseudo-code for f_0 is shown. The code for f_1 works analogously, only the arrays are complex-valued and additional arrays are used for the exponential functions, as these are repeatedly needed in the convolution.

```
def main():
    init()
    N = N_double
    h = h_min
    dN = 0
    # iterate over decimations
    for i in xrange(m_stop + 1):
        if i == m_stop:
            N = N_final
        new_stepwidth()
        calc_f0()
        h = 2*h
        dN = (dN + N + 1)//2

def new_stepwidth():
    # read in and interpolate for new step-size
    phi_eq, dphi_eq = init_eq()
    phi_eq[0] = 1
    dphi_eq[0] = -1
    m_eq = v1*phi_eq + v2*phi_eq**2
    # decimate
    f0[:dN] = f0_old[::2]
    m0[:dN] = m0_old[::2]
```

```
def calc_f0():
    if dN==0:
        # init first two values with 0
        initialval_f0()
    for i in xrange(dN, dN + N):
        if i == 0 or i == 1: continue
        g1 = 1. + v1 + v2
        g1 += v2*(phi_eq[1]**2 - phi_eq[0]**2)
        # accounting for end points of convolution
        g1 += 2.*(v1+v2*phi_eq[i])*(phi_eq[1] - phi_eq[0])
        g2 = (v1 + v2*phi_eq[i]) * phi_eq[i]
            * cos(omega*h*i) * (phi_eq[1] - phi_eq[0])
        g2 += (2. - cos(omega*h*i))*(dphi_eq[i] + phi_eq[i])
        # convolution
        for j in xrange(1,i):
            g2 += (phi_eq[j+1] - phi_eq[j])
                * (m[i-j] + v2*f0[i-j]*(phi_eq[j+1] + phi_eq[j]))
        # derivative
        Delta = 1./h * (1./2. * f0[i-2] - 2. * f0[i-1])
        Deltai = 3./(2.*h)
        f0[i] = -(g2 + Delta) / (g1 + Deltai)
        m[i] = m0(v1, v2, omega, h*i, f0[i], phi_eq[i])
```

C. Additional numerical results

As the discussion in the main part of the thesis concentrated on f_0, in this part two additional figures of numerical solutions of the Taylor approximation for f_1 are shown.

Also, the step-size analysis to show that the numerical solution does in fact converge against the analytical limits is completed here by figures for the convergence of f_1 and for f_0 and f_1 for a different set of parameter values.

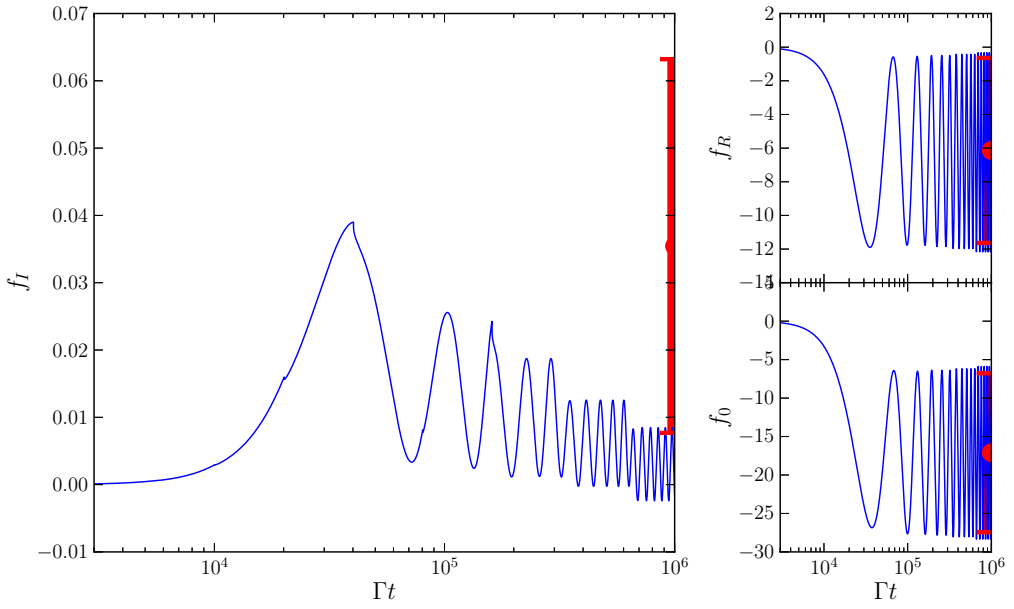

Figure C.0.1.: Numerical solution for f_I for $\epsilon = 0.001$, $\omega = 1e-4$, $N_{minp} = 100$. For comparison, f_R and f_0 are given as well. While the relative error of the long-time oscillation is small for f_R and f_0, f_I shows a large deviation, both in the offset and the oscillation amplitude. Visible changes of the solution at the changes of step-size starts right after the onset of the oscillation. The difference might be so obvious because the absolute size of f_I is rather small in comparison to the real part.

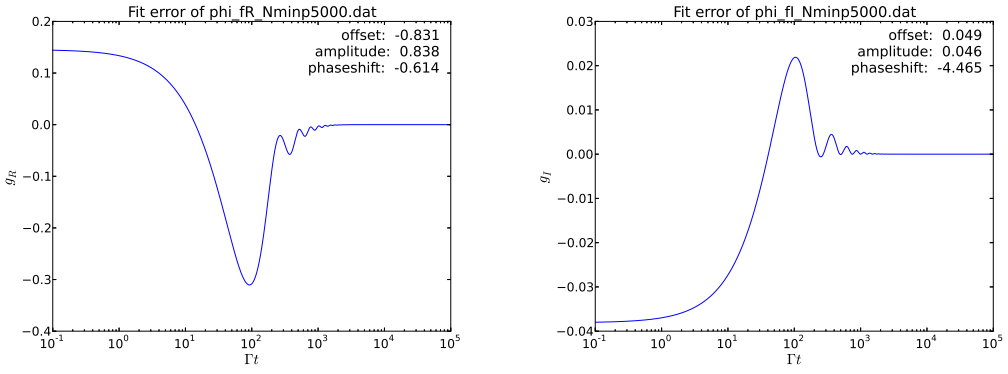

(a) Real part

(b) Imaginary part

Figure C.0.2.: Real and imaginary part of f_1 without the long-time limit

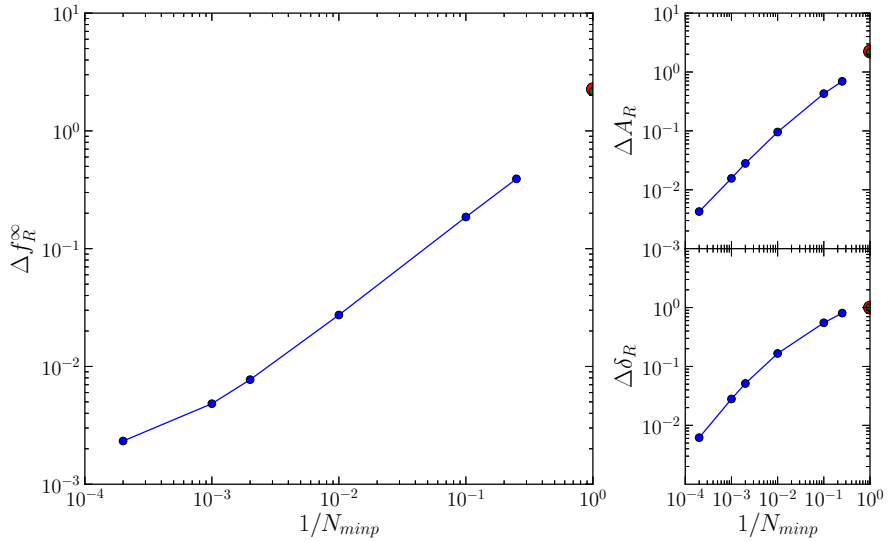

Figure C.0.3.: $f_R(\omega = 0.025, \epsilon = 0.01)$: Error of numeric value relative to analytic value of offset, amplitude and phase shift of oscillation for long times (10^5) as function of $1/N_{minp}$. Green dot at $1/N_{minp} = 1$: infinitely increasing step size (measured at $t = 10^8$), red dots: analytically expected values for $h_{max} \to \infty$ ($\omega \to 0$)

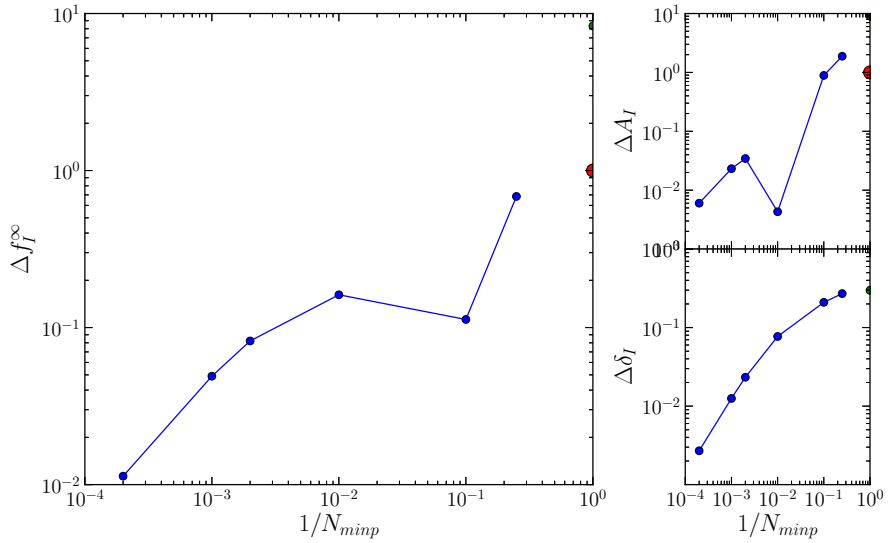

Figure C.0.4.: $f_I(\omega = 0.025, \epsilon = 0.01)$: Error of numeric value relative to analytic value of offset, amplitude and phase shift of oscillation for long times (10^5) as function of $1/N_{minp}$. Green dot at $1/N_{minp} = 1$: infinitely increasing step size (measured at $t = 10^8$), red dots: analytically expected values for $h_{max} \to \infty$ ($\omega \to 0$)

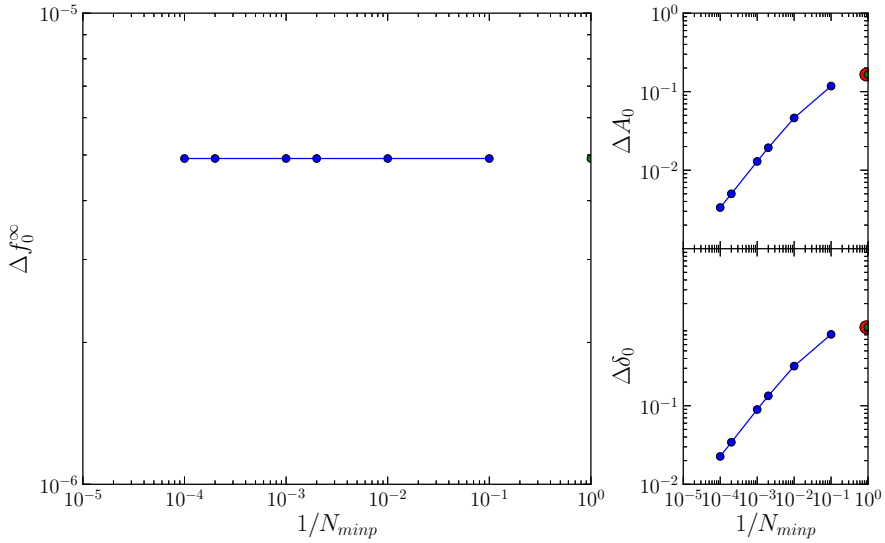

Figure C.0.5.: $f_0(\omega = 10^{-6}, \epsilon = 0.0001)$: Error of numeric value relative to analytic value of offset, amplitude and phase shift of oscillation for long times (10^5) as function of $1/N_{minp}$. Green dot at $1/N_{minp} = 1$: infinitely increasing step size (measured at $t = 10^{11}$).

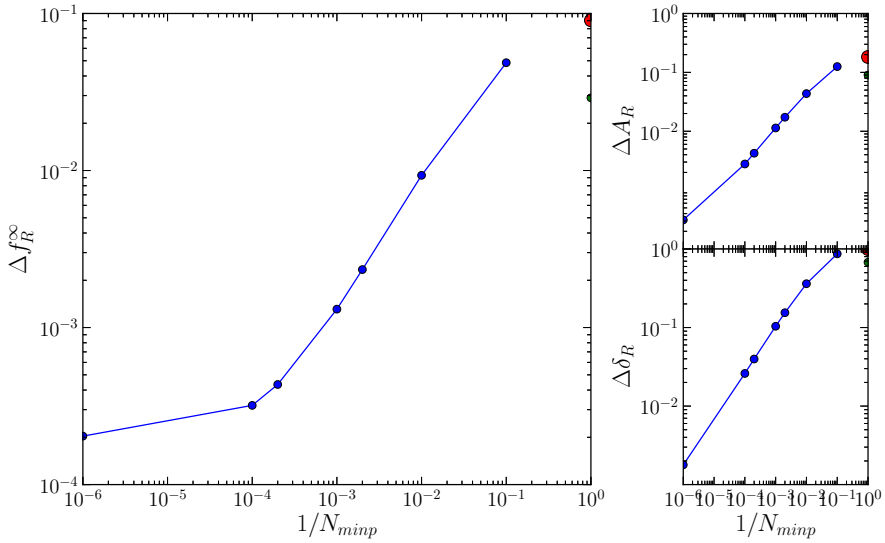

Figure C.0.6.: $f_R(\omega = 10^{-6}, \epsilon = 0.0001)$: Error of numeric value relative to analytic value of offset, amplitude and phase shift of oscillation for long times (10^5) as function of $1/N_{minp}$. Green dot at $1/N_{minp} = 1$: infinitely increasing step size (measured at $t = 10^8$), red dots: analytically expected values for $h_{max} \to \infty$ ($\omega \to 0$)

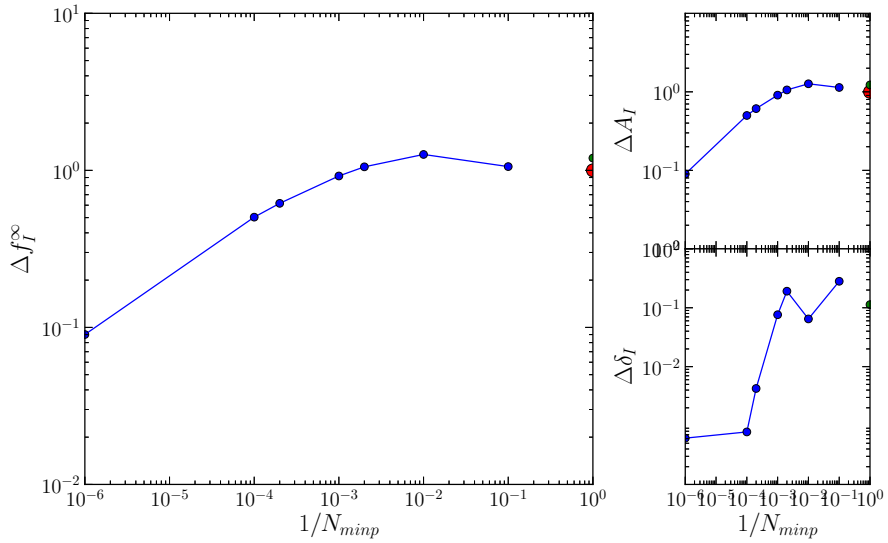

Figure C.0.7.: $f_I(\omega = 10^{-6}, \epsilon = 0.0001)$: Error of numeric value relative to analytic value of offset, amplitude and phase shift of oscillation for long times (10^5) as function of $1/N_{minp}$. Green dot at $1/N_{minp} = 1$: infinitely increasing step size (measured at $t = 10^8$), red dots: analytically expected values for $h_{max} \to \infty$ ($\omega \to 0$)

Acknowledgments

I would like to thank all the people who helped me during this year, my friends and my family – there are too many to name all here.
Also, many thanks to Thomas Voigtmann, whose tricks for numerics of schematic MCT equations made my code work, Fabian Frahsa for helpful discussions and Joe Brader for his code of the full schematic model.
But most of all, I want to thank Matthias Fuchs for giving me so many possibilities to look beyond the actual topic of my thesis and see all the fascinating different aspects of soft matter and glassy physics.

Bibliography

[1] Christian P. Amann, Miriam Siebenbüger, Matthias Krüger, Fabian Weysser, Matthias Ballauff, and Matthias Fuchs. Overshoots in stress-strain curves: Colloid experiments and schematic mode coupling theory. *Journal of Rheology*, 57(1):149, 2013.

[2] U Bengtzelius, W Götze, and A Sjölander. Dynamics of supercooled liquids and the glass transition. *Journal of Physics C: Solid State Physics*, 17(33):5915, 1984.

[3] J. Brader, M. Cates, and M. Fuchs. First-Principles Constitutive Equation for Suspension Rheology. *Physical Review Letters*, 101(13):1–4, September 2008.

[4] J. Brader, M. Siebenbürger, M. Ballauff, K. Reinheimer, M. Wilhelm, S. Frey, F. Weysser, and M. Fuchs. Nonlinear response of dense colloidal suspensions under oscillatory shear: Mode-coupling theory and Fourier transform rheology experiments. *Physical Review E*, 82(6):1–20, December 2010.

[5] Joseph M Brader, Thomas Voigtmann, Matthias Fuchs, Ronald G Larson, and Michael E Cates. Glass rheology : From mode-coupling theory to a dynamical yield criterion. 2009.

[6] T Franosch, M Fuchs, W Goetze, M R Mayr, A P Singh, W Götze, and W Go. Asymptotic laws and preasymptotic correction formulas for the relaxation near glass-transition singularities. *Phys. Rev. E*, 55(6):7153–7176, June 1997.

[7] M Fuchs. Nonlinear Rheological Properties of Dense Colloidal Dispersions Close to a Glass Transition Under Steady Shear. *Adv Polym Sci*, 236:55–115, 2009.

[8] M Fuchs. Notes on Structure and correlation functions, density functional and mode coupling theory, and rheology, 2011.

[9] Matthias Fuchs. Nonlinear Rheological Properties of Dense Colloidal Dispersions Close to a Glass Transition Under Steady Shear. (December 2009):55–115, 2010.

[10] Matthias Fuchs and Matthias Ballauff. Flow curves of dense colloidal dispersions: schematic model analysis of the shear-dependent viscosity near the colloidal glass transition. *The Journal of chemical physics*, 122(9):094707, March 2005.

[11] Matthias Fuchs and Michael E. Cates. Theory of Nonlinear Rheology and Yielding of Dense Colloidal Suspensions. *Physical Review Letters*, 89(24):7–10, November 2002.

[12] Matthias Fuchs and Michael E. Cates. Schematic models for dynamic yielding of sheared colloidal glasses. *Faraday Discussions*, 123:267–286, January 2003.

[13] M. V. Gnann, I. Gazuz, a. M. Puertas, M. Fuchs, and Th. Voigtmann. Schematic models for active nonlinear microrheology. *Soft Matter*, 7(4):1390, 2011.

[14] W Götze. *Complex Dynamics of Glass-Forming Liquids, A Mode-Coupling Theory*. Oxford University Press, 2009.

[15] W Gotze and L Sjogren. Relaxation processes in supercooled liquids. *Reports on Progress in Physics*, 241, 1992.

[16] W Götze and L Sjögren. Comments on the mode coupling theory for structural relaxation. *Chemical physics*, 212:47–59, 1996.

[17] W. Götze and Th. Voigtmann. Effect of composition changes on the structural relaxation of a binary mixture. *Phys. Rev. E*, 67(2):21502, February 2003.

[18] D. Hajnal and M. Fuchs. Flow curves of colloidal dispersions close to the glass transition. *The European Physical Journal E*, 28(2):125–138, September 2008.

[19] David Hajnal. Scaling laws in the rheology of colloidal dispersions by. Diplomarbeit, 2007.

[20] CJ Harrer and AM Puertas. Probability densities of a forced probe particle in glass: results from mode coupling theory and simulations of active microrheology. *arXiv preprint arXiv: ...*, 2012.

[21] H. Hayakawa and M. Otsuki. Mode-Coupling Theory of Sheared Dense Granular Liquids. *Progress of Theoretical Physics*, 119(3):381–402, March 2008.

[22] Oliver Henrich, Fabian Weysser, Michael E. Cates, and Matthias Fuchs. Hard discs under steady shear: comparison of Brownian dynamics simulations and mode coupling theory. *Philosophical Transactions of the Royal Society A: Mathematical, Physical and Engineering Sciences*, 367(1909):5033–5050, November 2009.

[23] JB Jones, JV Sanders, and ER Segnit. Structure of opal. 1964.

[24] V Krakoviack. Liquid-glass transition of confined fluids: insights from a mode-coupling theory. *Journal of Physics: Condensed Matter*, 17(45):S3565–S3570, November 2005.

[25] G Nägele and J Bergenholtz. Linear viscoelasticity of colloidal mixtures. *The Journal of Chemical Physics*, 108(23):9893–9904, 1998.

[26] Roberto Piazza. *Soft Matter*. Springer Italia.

[27] Rabea Seyboldt. Shear moduli of two dimensional colloidal mixtures. Bachelorarbeit, 2011.

[28] Marco Tarzia, Giulio Biroli, Alexandre Lefèvre, and Jean-philippe Bouchaud. Anomalous nonlinear response of glassy liquids : General arguments and a mode-coupling approach. *Journal of Chemical Physics*, 054501, 2010.

[29] Th. Voigtmann, J. M. Brader, M. Fuchs, and M. E. Cates. Schematic mode coupling theory of glass rheology: single and double step strains. *Soft Matter*, 8(15):4244, 2012.

[30] Thomas Voigtmann. Schematische Modelle der Modenkopplungstheorie mit Hopping-Term. Diplomarbeit, 1998.

[31] F. Weysser, a. Puertas, M. Fuchs, and Th. Voigtmann. Structural relaxation of polydisperse hard spheres: Comparison of the mode-coupling theory to a Langevin dynamics simulation. *Physical Review E*, 82(1):1–21, July 2010.

[32] J Zausch, J Horbach, M Laurati, S U Egelhaaf, J M Brader, Th Voigtmann, and M Fuchs. From equilibrium to steady state: the transient dynamics of colloidal liquids under shear. *Journal of Physics: Condensed Matter*, 20(40):404210, October 2008.